J. Fluid Mech. (1998), *vol.* 362, *pp.* 83–119. Printed in the United Kingdom

The growth, saturation, and scaling behaviour of one- and two-dimensional disturbances in fluidized beds

By M. F. GÖZ† AND S. SUNDARESAN

Department of Chemical Engineering, Princeton University,
Princeton, NJ 08544, USA

(Received 10 July 1997, and in revised form 30 December 1997)

It is well-known that fluidized beds are usually unstable to small perturbations and that this leads to the primary bifurcation of vertically travelling plane wavetrains. These one-dimensional periodic waves have been shown recently to be unstable to two-dimensional perturbations of large transverse wavelength in gas-fluidized beds. Here, this result is generalized to include liquid-fluidized beds and to compare typical beds fluidized with either air or water. It is shown that the instability mechanism remains the same but there are big differences in the ratio of the primary and secondary growth rates in the two cases. The tendency is that the secondary growth rates, scaled with the amplitude of a fully developed plane wave, are of similar magnitude for both gas- and liquid-fluidized beds, while the primary growth rate is much larger in the gas-fluidized bed. This means that the secondary instability is accordingly stronger than the primary instability in the liquid-fluidized bed, and consequently sets in at a much smaller amplitude of the primary wave. However, since the waves in the liquid-fluidized bed develop on a larger time and length scale, the primary perturbations need longer time and thereby travel farther until they reach the critical amplitude. Which patterns are more amenable to being visually recognized depends on the magnitude of the initially imposed disturbance and the dimensions of the apparatus. This difference in scale plays a key role in bringing about the differences between gas- and liquid-fluidized beds; it is produced mainly by the different values of the Froude number.

1. Introduction

Puzzling differences in the behaviour of particle assemblies fluidized uniformly by a gas or a liquid have concerned researchers for decades. While the first impression was that only fluidization with a gas leads to bubbling behaviour, it was found later that this phenomenon can also occur in liquid-fluidized beds (Didwania & Homsy 1981). On the other hand, liquid-fluidized beds seemed to favour more modest wave patterns in the form of one- and multi-dimensional travelling waves (El-Kaissy & Homsy 1976). In fact, the observation of plane wavetrains moving steadily through the bed while acquiring transverse structure triggered the suspicion that both two-dimensional waves and bubbles might result from a secondary instability at which

† Author to whom correspondence should be addressed; present address: Martin-Luther-Universität Halle-Wittenberg, FB Verfahrenstechnik, MVT/UST, D-06099 Halle, Germany.

the primarily unstable vertically travelling one-dimensional wave is overtaken by a more complex pattern. To some extent, this corresponded neatly with theoretical considerations based on volume-averaged equations of motion for the particle and fluid phases which predicted that a uniformly fluidized suspension is most unstable to one-dimensional perturbations (Anderson & Jackson 1968) and that this leads to the onset of periodic travelling plane waves (Needham & Merkin 1986). It was also encouraging to find (Anderson & Jackson 1968) that the growth rate of initial perturbations is typically much higher in gas-fluidized beds which would lead to faster development of concentration gradients in them. But most of the subsequent analytical studies were restricted to one-dimensional treatments and thus could not address the question of a secondary, transverse instability, nor were multi-dimensional numerical computations (e.g. Pritchett, Blake & Garg 1978; Kuipers, Prins & van Swaaij 1991; Hernández & Jiménez 1991) able to resolve the origin of such a transition or to explain the mentioned differences. So the major questions remained: is the usual modelling able to account for these differences and where do they come from?

The problem of a secondary instability involving the transition from a one- to a two-dimensional pattern in fluidized beds and other multi-phase flows has been attacked recently with various approaches. Batchelor (1993) has related the secondary instability in a gas-fluidized bed to the overturning instability of an unbounded stratified fluid (Batchelor & Nitsche 1991). Göz has analysed primary bifurcations of two-dimensional travelling waves directly from the uniform state (1992, 1995*a*) and investigated vertically and oblique travelling waves in detail (1993*a*, *b*), finding only minor differences between gas- and liquid-fluidized beds. He then (1995*c*) showed the relevance of these primary two-dimensional waves and that of pure transverse perturbation modes of the uniform state to the onset of a secondary instability in gas-fluidized beds, as one or two of these modes become unstable when the amplitude of the plane wavetrain exceeds a threshold proportional to the square of the transverse wavenumber. In another study Göz (1995*b*) considered a small Froude number approximation to two-dimensional multi-phase flows and found that gas- and liquid-fluidized beds exhibited similar bifurcation behaviour. The differences between gas- and liquid-fluidized beds are therefore not likely to be manifested through a qualitatively different bifurcation structure; quantitative differences in the length and time scales associated with these beds are likely to play an important role in distinguishing between bubbling and non-bubbling systems. It was indeed noted by Anderson, Sundaresan & Jackson (1995) that the growth rate of primary, one-dimensional disturbances from an unstable uniform state in a bubbling system is comparable to that of secondary, two-dimensional perturbations from a fully developed one-dimensional travelling wave, while in non-bubbling systems the former growth rate is significantly smaller than the latter. One can readily appreciate why this difference in the relative growth rates will influence the manner in which high-amplitude two-dimensional travelling waves evolve from an unstable uniform state; but it is hardly obvious why relative growth rates determine whether a given system will bubble or not.

Glasser, Kevrekidis & Sundaresan (1996, 1997) found through numerical bifurcation analysis that the principal behaviour of beds fluidized with water or air is the same; in both cases one obtains a transition from the state of uniform fluidization to a one- and then a two-dimensional vertical travelling wave with a bubble-like structure. They noted that in some solutions containing a bubble-like hole the particles accelerate as they enter the hole through the roof and decelerate as they exit the hole at the bottom, while in others the particles experience an additional stage of deceleration

and re-acceleration. Although both types of solutions were found to be locally stable, solutions of the former type evolved smoothly in transient integration of the equations of motion when an unstable uniform state or one-dimensional travelling wave was subjected to a two-dimensional perturbation. In the latter case the transients neither reached the fully developed bubble-like solution nor did they settle down into any regular pattern. These authors proposed that fluidized systems whose fully developed bubble-like solutions belong to this latter type be labelled as non-bubbling. Interestingly, they found that the relative growth rate criterion suggested by Anderson *et al.* (1995) is indeed a good indicator as to whether a system will bubble or not. These observations suggest a closer look at the growth rates of the primary and secondary instabilities in an attempt to elucidate the appropriate scales for these quantities.

With this in mind, we extend the previous analysis of Göz (1995*c*) to liquid-fluidized beds by incorporating the terms accounting for fluid inertia and viscosity in the momentum equation for the continous phase. We shall see that the instability mechanism is the same for both gas- and liquid-fluidized beds. Having thus ruled out qualitative differences between gas- and liquid-fluidized beds in our model we look for quantitative discrepancies. We discuss various examples and find that for typical parameters of air- and water-fluidized beds the secondary growth rates, scaled with the amplitude of quasi-steady plane waves, are of comparable magnitude, in stark contrast to the primary rates. In the cases considered the secondary instability is stronger than the primary instability in the water-fluidized bed, and overwhelms the plane wave at a smaller amplitude. But because the waves in the water-fluidized bed grow more slowly, they need more time and space to develop, so that there is a better chance to observe the rise of plane waves and the development of two-dimensional structures – if the vessel is large enough. On the other hand, if disturbances imposed at, for instance, the orifices at the bottom of the bed are as large as the critical amplitude, two-dimensional patterns will be observed right away.

The time and length scales depend on the fluidization velocity, which can easily change by one or two orders of magnitude with greatly varying bed parameters; this affects the two basic non-dimensional parameters in our model, namely the Froude and the Reynolds numbers. Compared to that, the often neglected terms describing fluid inertia and viscosity in the momentum equation for the continous phase seem to be of less importance. Although the analysis presented here does not go beyond the point of onset of a secondary bifurcation and thus does not allow any solid conclusion about the formation of stable two-dimensional travelling waves, it points in the same direction as the studies by Anderson *et al.* (1995) and Glasser (1996). In these we may see a confirmation of the empirical criterion of Wilhelm & Kwauk (1948) that beds with large Froude number bubble while beds with small Froude number do not (our Froude number is based on the velocity of uniform fluidization at a certain voidage value and the particle radius). The important parameter behind this is the (square of the) fluidization velocity u_0. An asymptotic analysis near the stability limit carried out in the present study reveals that the maximum dimensionless primary growth rate is proportional to the Reynolds number, so that the magnitude of the dimensional growth rate is determined by the strength of the instability and the value of $\rho_s u_0^2/\mu_s^0$, which is proportional to the Froude number. Here ρ_s is the particle density and μ_s^0 is the viscosity of the particulate phase. The large differences between the primary growth rates in air- and water-fluidized beds are then readily explained in terms of this scale. The situation is more involved with the secondary growth rates, but based on another asymptotic analysis for small transverse wavenumbers we have derived

an approximate expression for the maximum (dimensional) secondary growth rates and shown that their values stay within the same order of magnitude over the whole range of Froude numbers of practical interest (i.e. except for extremely small or large Froude numbers).

The present paper, devoted primarily to a study of the stability of plane waves to two-dimensional perturbations employing a Fourier decomposition, is structured as follows. We begin by writing the equations of motion in perturbation form around the uniform base state and decomposing the nonlinear expressions into quadratic and higher-order terms (§2). This enables us to derive a scalar equation in which the linear part operates on the voidage variable only, and similarly simple-in-structure equations for the other variables. In §3 we consider the linear problems, first around the uniform state, then around a growing one-dimensional wave. We derive an approximate expression for the maximum growth rate of weakly unstable beds which reveals $\rho_s u_0^2/\mu_s^0$ as the correct scale for the growth rate (§3.1). Next we break down the equations for the linear stability of small-amplitude one-dimensional waves into equations for the harmonic components of all variables (§3.2) and derive three coupled equations for the basic Fourier components of the voidage by eliminating the other variables (§3.3). These equations are solved for small times giving an indication of the initial secondary growth rates. The approximation becomes unreliable for larger amplitudes of the primary disturbance and also shows a singularity for vanishing transverse wavenumber. This necessitates a rescaling of the secondary growth rate and the transverse wavenumber with the amplitude of the plane wave (§4). For typical parameters it turns out that the scaled secondary growth rates are of comparable magnitude for both gas- and liquid-fluidized beds. In §5 we derive approximate expressions for secondary growth rates, critical amplitudes, and length and time scales, and evaluate their Froude number scaling. Section 6 contains our conclusions.

2. Equations of motion in perturbation form

We will begin with a description of the volume-averaged equations of motion for the fluid and particle phases cast in a dimensionless form (§2.1). For the purpose of the present study, it is convenient to rewrite these equations in the form of a perturbation of a uniformly fluidized state (§2.2).

2.1. *Volume-averaged equations of motion*

The volume-averaged equations of motion for fluidized beds (Anderson & Jackson 1968), when formulated in a frame moving vertically upwards with constant velocity ω (Göz 1992, 1995*c*), take the form

$$-\partial_t\phi + \nabla\cdot[(1-\phi)(\boldsymbol{v}-\omega\boldsymbol{k})] = 0, \tag{2.1a}$$

$$\partial_t\phi + \nabla\cdot[\phi(\boldsymbol{u}-\omega\boldsymbol{k})] = 0, \tag{2.1b}$$

$$F(1-\phi)[\partial_t\boldsymbol{v} + (\boldsymbol{v}-\omega\boldsymbol{k})\cdot\nabla\boldsymbol{v}] = -(1-\phi)\boldsymbol{k} + B(\phi)(\boldsymbol{u}-\boldsymbol{v}) - \nabla\cdot\boldsymbol{\sigma}_s - (1-\phi)\nabla p + \alpha_1 v\mu(1-\phi)(\Delta + \bar{\kappa}\nabla\nabla\cdot)\boldsymbol{u}, \tag{2.1c}$$

$$F\delta\phi[\partial_t\boldsymbol{u} + (\boldsymbol{u}-\omega\boldsymbol{k})\cdot\nabla\boldsymbol{u}] = -\delta\phi\boldsymbol{k} - B(\phi)(\boldsymbol{u}-\boldsymbol{v}) - \phi\nabla p + v\mu[1-\alpha_2(1-\phi)](\Delta + \bar{\kappa}\nabla\nabla\cdot)\boldsymbol{u}. \tag{2.1d}$$

The variables are the fluid (liquid or gas) volume fraction or voidage ϕ, the effective fluid pressure p, and the laboratory-frame particle- and fluid-phase velocities $\boldsymbol{v}$ and $\boldsymbol{u}$, respectively. Such a 'mixed' representation using a moving coordinate system and a different frame of reference for calculating the velocities is unconventional but useful

for the purpose of the present study as it introduces the wave speed ω, which we will use as the control or bifurcation parameter. The second lines in (2.1c, d) account for the contributions of the stress tensor of the fluid phase; since the fluid is assumed to be incompressible, its pressure has to be determined as part of the solution. We assume a Newtonian form for the stress tensor of the solid phase, i.e.

$$\boldsymbol{\sigma}_s = p_s \boldsymbol{I} - \frac{\mu}{\mu_s^0} \{\lambda_s(\phi)(\nabla \cdot \boldsymbol{v})\boldsymbol{I} + \mu_s(\phi)[\nabla \boldsymbol{v} + (\nabla \boldsymbol{v})^T - \tfrac{2}{3}(\nabla \cdot \boldsymbol{v})\boldsymbol{I}]\}, \tag{2.1e}$$

and write

$$\nabla p_s(\phi) = G(\phi)\nabla\phi \quad \text{with} \quad 0 > p_s'(\phi) = G(\phi), \tag{2.1f}$$

taking p_s to be a monotonically decreasing function of the voidage. Specifically, we assume

$$p_s(\phi) = g_0 \frac{(1-\phi)^{m_1}}{(\phi - \phi_{cp})^{m_2}} \tag{2.1g}$$

with $m_1 = 1$ and either $m_2 = 0$ ($\Rightarrow\ G \equiv -g_0$) or $m_2 = 2$ ($\Rightarrow\ G' > 0$); the close packing limit is taken to be $\phi_{cp} = 0.35$. In most of the examples discussed in the present paper, we will assume that $m_1 = 1$ and $m_2 = 0$, as it is now well established that such a linear closure for p_s is enough to capture phenomena such as the existence of a small region of stable uniform fluidization, the birth of one-dimensional vertically travelling waves through the loss of stability of this uniformly fluidized state (Needham & Merkin 1986; Göz 1993*b*), and the emergence of two-dimensional travelling waves having a bubble-like hole from the one-dimensional waves (Göz 1995*c*; Glasser *et al.* 1996, 1997). As nonlinear expressions for $p_s(\phi)$ are frequently used in the literature (for example, see Anderson *et al.* 1995), we will occasionally touch upon the implications of such a nonlinearity for the secondary instability by considering the case of $m_1 = 1$ and $m_2 = 2$.

The equations have been made dimensionless by using the particle radius r_p as length scale and the fluidization velocity $\boldsymbol{u}_0 = u_0\boldsymbol{k}$ as the basis for the velocity and time (r_p/u_0) scales. Here $\boldsymbol{k}$ is the unit vector parallel to the z-axis pointing against gravity; the transverse direction will be denoted by y. Both effective pressure p and bulk modulus/interparticle pressure $G(\phi)$ have been rescaled with $\rho_s g r_p$, where g is the acceleration due to gravity and ρ_s represents the density of the particles. The density ratio of the two phases is denoted by $\delta = \rho_f/\rho_s$, and the ratio of the shear viscosity coefficients is given by $\nu = \mu_f/\mu_s^0$, where $\mu_s^0 = \mu_s(\phi_0)$. The shear and bulk viscosity coefficients of the particulate phase, μ_s and λ_s respectively, may depend on the voidage. Thus we end up with the non-dimensional parameters $F = u_0^2/(gr_p)$, δ, ν, and a particle-based Reynolds number $R = \rho_s u_0 r_p/\mu_s^0$. In addition, we introduce the coefficients $\mu = F/R$, $\kappa = (\lambda_s^0 + \mu_s^0/3)/\mu_s^0$ and $\bar{\kappa} = (\lambda_f + \mu_f/3)/\mu_f$. Within this scaling, the drag coefficient is assumed to be of the form

$$B(\phi) = \tfrac{9}{2}\,\nu\mu\frac{1-\phi}{\phi^n}. \tag{2.2}$$

The exponent n depends on the Reynolds number for fluid flow around an isolated particle settling under gravity (Richardson & Zaki 1954) and n is approximately equal to 3 when this Reynolds number is small. Equations (2.1) admit as a solution the uniformly fluidized state

$$\phi = \phi_0, \quad \boldsymbol{v} = 0, \quad \boldsymbol{u}_0 = \boldsymbol{k}, \quad \nabla p_0 = -[1 - \phi_0(1-\delta)]\,\boldsymbol{k} \equiv p_0'\boldsymbol{k}, \tag{2.3}$$

and it can be readily shown that

$$\phi_0^{n+1} = \frac{9}{2}\frac{\nu\mu}{1-\delta}, \quad B_0 \equiv B(\phi_0) = (1-\delta)\phi_0(1-\phi_0). \tag{2.4}$$

We have written the equations in such a way that they reduce to the system of equations analysed by Göz (1992) for $\alpha_{1,2} = 0$ (i.e. $\alpha_1 = \alpha_2 = 0$), and to that studied by Glasser *et al.* (1996, 1997) for $\alpha_{1,2} = 1$, thus making comparisons as straightforward as possible. Note that in the latter papers the voidage is given by $1-\phi$, the effective fluid pressure is denoted by p_f, and the bulk viscosity coefficients are taken to be zero, so that $\kappa = \bar{\kappa} = 1/3$.

The problem of general closure for the locally averaged equations of motion remains unsolved. In spite of this, it is now clear that very simple, physically credible closure relations, such as the ones described above, suffice to distinguish between bubbling and non-bubbling systems. The model analysed in this study is by no means complete; for example, it does not consider the virtual mass effect which may become important in liquid-fluidized beds. We have not included this effect, as it has already been shown by Anderson *et al.* (1995) and Glasser *et al.* (1996, 1997) that a distinction between bubbling and non-bubbling systems is possible even if one neglects the virtual mass term; that is, the effect of the virtual mass term is only quantitative and not qualitative. Furthermore, the virtual mass term has very little effect on the occurrence of the primary instability, and we expect it to play a minor (quantitative) role for our results. In addition, we want to compare the outcome of the analysis to the previously mentioned numerical studies without virtual mass which showed the sought-for distinction between bubbling and non-bubbling systems. It is for these reasons that we have not included the virtual mass term in the present analysis. On similar grounds, we have neglected a possible dependence of both the drag and viscosity coefficients on the relative velocity of the two phases.

2.2. *Equations in terms of deviation variables*

In order to get the most general and transparent approach to the treatment of the nonlinear problem, we rewrite the equations (2.1) in form of a perturbation of the uniform state, i.e.

$$\phi = \phi_0 + \tilde{\phi}, \quad p = p_0 + \tilde{p}, \quad \boldsymbol{v} = \tilde{\boldsymbol{v}}, \quad \boldsymbol{u} = \boldsymbol{k} + \tilde{\boldsymbol{u}}, \tag{2.5}$$

and move all nonlinear terms to the right-hand sides. This will produce a system of equations in terms of the perturbation variables ((2.6*a–d*) below), which we will combine to produce a scalar equation in which the linear terms contain the voidage only ((2.8) below). Similarly, we can derive equations whose linear parts couple the pressure with the voidage (2.7), and the velocities with voidage and pressure (2.10) and (2.11), respectively; of course, the nonlinear terms still contain all the variables. This formulation has the advantage of a maximal decoupling of the variables (corresponding to a 'diagonalization' of the system of equations) and highlights the role of the voidage variable.

Expanding the coefficients B and G and retaining cubic terms, we obtain the following set of equations:

$$-\partial_t\tilde{\phi} + (1-\phi_0)\,\nabla\cdot\tilde{\boldsymbol{v}} + \omega\partial_z\tilde{\phi} = \nabla\cdot(\tilde{\phi}\tilde{\boldsymbol{v}}) \equiv R_1, \tag{2.6a}$$

$$\partial_t\tilde{\phi} + \phi_0\,\nabla\cdot\tilde{\boldsymbol{u}} + (1-\omega)\partial_z\tilde{\phi} = -\nabla\cdot(\tilde{\phi}\tilde{\boldsymbol{u}}) \equiv R_2, \tag{2.6b}$$

$$F(1-\phi_0)(\partial_t\tilde{\boldsymbol{v}} - \omega\partial_z\tilde{\boldsymbol{v}}) - \mu(\Delta + \kappa\nabla\nabla\cdot)\tilde{\boldsymbol{v}} - B_0(\tilde{\boldsymbol{u}} - \tilde{\boldsymbol{v}}) - b_1\,\tilde{\phi}\,\boldsymbol{k} + G_0\nabla\tilde{\phi} + (1-\phi_0)\nabla\tilde{p} - \nu_1(\Delta + \bar{\kappa}\nabla\nabla\cdot)\tilde{\boldsymbol{u}} = \boldsymbol{R}_3, \tag{2.6c}$$

$$F\delta\phi_0[\partial_t\tilde{\boldsymbol{u}} + (1-\omega)\partial_z\tilde{\boldsymbol{u}}] - v_2(\Delta + \bar{\kappa}\nabla\nabla\cdot)\tilde{\boldsymbol{u}} + B_0(\tilde{\boldsymbol{u}} - \tilde{\boldsymbol{v}}) + b_\delta\,\tilde{\phi}\,\boldsymbol{k} + \phi_0\nabla\tilde{p} = \boldsymbol{R}_4\,, \quad (2.6d)$$

with the obvious notation $B_0 = B(\phi_0)$, $B_0' = B'(\phi_0)$, etc.; nonlinear terms like $\boldsymbol{R}_{3,4}$ and constants like $b_{1,\delta}$, $v_{1,2}$ will be given in Appendix A.

Upon taking the divergence of (2.6*c*) and inserting (2.6*a*, *b*), an equation for the pressure is obtained, in which the linear terms depend on the voidage only:

$$\begin{aligned}(1-\phi_0)\Delta\tilde{p} = {} & -F\ddot{\tilde{\phi}} + 2F\omega\dot{\tilde{\phi}}' - G_0\Delta\tilde{\phi} - F\omega^2\tilde{\phi}'' - FE\dot{\tilde{\phi}} \\ & + [b_1 - FE(1-\phi_0-\omega)]\,\tilde{\phi}' - (c_1\omega + \alpha_1 FH)\Delta\tilde{\phi}' + c_1\Delta\dot{\tilde{\phi}} + R_p\,, \quad (2.7)\end{aligned}$$

where we have denoted the time derivative with a dot and the derivative with respect to z with a prime. For R_p, c_1, E, H see Appendix A.

The same can be done with (2.6*d*), so that by forming $\phi_0\nabla\cdot(2.6c) - (1-\phi_0)\nabla\cdot(2.6d)$ the linear pressure term is eliminated and *a scalar equation is obtained, in which the linear terms contain the voidage only*:

$$\mathrm{L}\,\tilde{\phi} = R_\phi(\tilde{\boldsymbol{U}})\,, \qquad \tilde{\boldsymbol{U}} = (\tilde{\phi}, \tilde{p}, \tilde{\boldsymbol{v}}, \tilde{\boldsymbol{u}})\,. \quad (2.8)$$

Here, L represents the linear operator

$$\begin{aligned}\mathrm{L} = {} & A\partial_t^2 + 2(C - A\omega)\partial_t\partial_z - M\Delta + (A\omega^2 - 2C\omega + C)\partial_z^2 \\ & + E\partial_t + (D - E\omega)\partial_z + (\tilde{J}\omega - \tilde{H})\Delta\partial_z - \tilde{J}\Delta\partial_t\,, \quad (2.9)\end{aligned}$$

while the nonlinear terms R_ϕ and the various constants are presented in Appendix A.

In addition, using again (2.6*a*, *b*), equations (2.6*c*) and (2.6*d*) may be rewritten as

$$\begin{aligned}& F(1-\phi_0)(\dot{\tilde{\boldsymbol{v}}} - \omega\tilde{\boldsymbol{v}}') - \mu\Delta\tilde{\boldsymbol{v}} - B_0(\tilde{\boldsymbol{u}} - \tilde{\boldsymbol{v}}) - v_1\Delta\tilde{\boldsymbol{u}} \\ & \qquad = b_1\,\tilde{\phi}\,\boldsymbol{k} - G_0\nabla\tilde{\phi} + \mu_1\nabla\dot{\tilde{\phi}} - \mu_2\nabla\tilde{\phi}' - (1-\phi_0)\nabla\tilde{p} + \boldsymbol{R}_{\boldsymbol{v}}\,, \quad (2.10) \\ & F\delta\phi_0[\dot{\tilde{\boldsymbol{u}}} + (1-\omega)\tilde{\boldsymbol{u}}'] - v_2\Delta\tilde{\boldsymbol{u}} + B_0(\tilde{\boldsymbol{u}} - \tilde{\boldsymbol{v}}) \\ & \qquad = -b_\delta\,\tilde{\phi}\,\boldsymbol{k} - \frac{v_2\bar{\kappa}}{\phi_0}\nabla[\dot{\tilde{\phi}} + (1-\omega)\tilde{\phi}'] - \phi_0\nabla\tilde{p} + \boldsymbol{R}_{\boldsymbol{u}}\,, \quad (2.11)\end{aligned}$$

where the nonlinear terms $\boldsymbol{R}_{\boldsymbol{v},\boldsymbol{u}}$ and the new constants $\mu_{1,2}$ can again be found in Appendix A.

If we assume that the perturbation from the uniform state is small, then we might be able to neglect most of the nonlinear terms in (2.7), (2.10) and (2.11), *so that these equations would determine pressure and velocities as an essentially linear functional of the voidage*. Inserting the results into the quadratic terms of (2.8) would allow us to eliminate the other variables up to this order of approximation, and would yield a better description of the behaviour of the voidage than the linearization around the uniform state. In fact, because we want to study the fate of two-dimensional perturbations of a growing or fully developed one-dimensional wave, and the analysis of Göz (1995*c*) for gas-fluidized beds (more precisely, $\delta = v = 0$ in (2.1*d*)) shows that for this purpose it is sufficient to obtain the leading-order approximations to the variables, we shall need only a few contributions from the quadratic terms in (2.7), (2.10) and (2.11).

3. The linearized problems

When the state of uniform fluidization becomes unstable, the fastest growing mode is a one-dimensional travelling wave whose wavefronts have no horizontal structure (Anderson & Jackson 1968). In this section, we outline the procedure adopted by us

to analyse these one-dimensional waves and revisit the problem of the linear stability of the uniform state to bring forth the origin of the large differences between the growth rates of these waves in typical gas- and liquid-fluidized beds (§3.1). We will then consider the problem of stability of these one-dimensional waves to transverse perturbations. The mathematical preliminaries for this analysis will be provided in §3.2. Section 3.3 will address the problem of the initial growth rate of transverse perturbations superimposed on growing one-dimensional waves.

We now seek an approximation of a one-dimensional solution $\boldsymbol{U}_1(z,t)$, which is assumed to be small, i.e. $\boldsymbol{U}_1 = \epsilon \boldsymbol{U}_{11} + O(\epsilon^2),\ \epsilon \ll 1$. Hence,

$$\mathrm{L}\phi_1 = \epsilon \mathrm{L}\phi_{11} + O(\epsilon^2) = R_\phi(\epsilon \boldsymbol{U}_{11} + O(\epsilon^2)) = O(\epsilon^2), \quad R_{p,\boldsymbol{v},\boldsymbol{u}}(\boldsymbol{U}_1) = O(\epsilon^2), \tag{3.1}$$

so that to leading order the linear problem $\mathrm{L}\phi_{11}(z,t) = 0$ has to be solved; then the other variables follow easily from the linear parts of (2.7), (2.10), (2.11).

Upon linearizing the equations around $\boldsymbol{U}_1$, we obtain

$$\mathrm{L}\phi = R'_\phi(\boldsymbol{U}_1) \cdot \boldsymbol{U}, \quad \text{with } R'_\phi(\boldsymbol{U}_1) = O(\epsilon),\ R'_{p,\boldsymbol{v},\boldsymbol{u}}(\boldsymbol{U}_1) = O(\epsilon),$$

so that we can utilize the approximation

$$\left.\begin{aligned} \mathrm{L}\phi &= \frac{\delta}{\delta \boldsymbol{U}} R_{\phi|_{\text{quadratic terms}}}(\epsilon \boldsymbol{U}_{11}) \cdot \boldsymbol{U} + O(\epsilon^2) \cdot \boldsymbol{U}, \\ R'_{p,\boldsymbol{v},\boldsymbol{u}}(\boldsymbol{U}_1) &= R'_{p,\boldsymbol{v},\boldsymbol{u}}(\epsilon \boldsymbol{U}_{11}) + O(\epsilon^2). \end{aligned}\right\} \tag{3.2}$$

In each case, our aim is to find simple relationships between the voidage and the remaining dependent variables, so that it is possible to replace them in (3.2) and get an equation for the voidage alone. This is straightforward in the first case, but requires a large amount of algebra in the second. Since only the quadratic terms play a role in (3.2), it will be sufficient to neglect most of the nonlinear terms in equations (2.7), (2.10), and (2.11).

3.1. *Approximation of one-dimensional solutions*

How to obtain an approximation of fully developed one-dimensional vertically travelling wave solutions has been demonstrated by Göz (1995*c*) for the much simpler case $\delta = \nu = 0$. However, it has been shown in the same paper that for the calculation of its transverse stability only the linear approximation is needed. Because we want to consider the initial stage of growing linear modes as well as the behaviour of two-dimensional perturbations of these modes, we combine the two approaches by writing

$$\phi_1 = \phi_+ \mathrm{e}^{\mathrm{i}\lambda z} + \phi_- \mathrm{e}^{-\mathrm{i}\lambda z}, \quad \phi_+ = v_p \mathrm{e}^{\sigma t},\ \phi_- = \bar{\phi}_+, \tag{3.3}$$

where we must assume $|\phi_+| \ll 1$. For convenience of notation we have replaced $\epsilon\phi_{11}$ by ϕ_1. Denoting the linear approximations to the vertical velocity components by v_1 and u_1 we obtain

$$(v,u,p)_1 = (v_1,u_1,p)_+ \mathrm{e}^{\mathrm{i}\lambda z} + (v_1,u_1,p)_- \mathrm{e}^{-\mathrm{i}\lambda z}, \tag{3.4a}$$

$$v_{1+} = \frac{\sigma - \mathrm{i}\lambda\omega}{\mathrm{i}\lambda(1-\phi_0)}\phi_+ = \bar{v}_{1-}, \quad p_+ = a\phi_+ = \bar{p}_-, \tag{3.4b}$$

$$u_{1+} = -\frac{\sigma + \mathrm{i}\lambda(1-\omega)}{\mathrm{i}\lambda\phi_0}\phi_+ = \bar{u}_{1-}, \tag{3.4c}$$

with

$$a = \frac{1}{\lambda^2(1-\phi_0)}\,[F(\sigma - \mathrm{i}\lambda\omega)^2 - G_0\lambda^2 + (\sigma - \mathrm{i}\lambda\omega)(c_1\lambda^2 + FE) + \mathrm{i}\lambda(B_0/\phi_0 - b_1 - \alpha_1 FH\lambda^2)]. \quad (3.5)$$

The eigenvalues are to be determined from the dispersion relation

$$A(\sigma - \mathrm{i}\lambda\omega)^2 + (\sigma - \mathrm{i}\lambda\omega)(E + 2\mathrm{i}C\lambda + \tilde{J}\lambda^2) + \mathrm{i}D\lambda + (M - C)\lambda^2 + \mathrm{i}\tilde{H}\lambda^3 = 0. \quad (3.6)$$

By setting $\omega = 0$ we obtain the usual and often studied eigenvalue problem for disturbances of the uniform state. Let us briefly recapitulate that the base state is linearly stable if the two conditions

$$f(d) \geqslant 0,\ f(h) \geqslant 0, \quad (3.7)$$

with

$$f(s) = m - c + 2cs - s^2,\ m = \frac{M}{A},\ c = \frac{C}{A},\ d = \frac{D}{E},\ h = \frac{\tilde{H}}{\tilde{J}},$$

are met, but that they are not independent of each other; if δ and ν are smaller than 1, which is the case here, then $d > h$ and $f(h) > f(d)$ (Göz 1992; Göz *et al.* 1996). The conditions (3.7) can be understood from the behaviour of the real part of σ for small (cf. Göz 1995*b*) and large wavenumbers, namely

$$\mathrm{Re}\,\sigma = -\frac{A}{E}f(d)\lambda^2 \pm O(\lambda^4),\ \lambda \ll 1;\ \mathrm{Re}\,\sigma \to -\frac{A}{\tilde{J}}f(h),\ \lambda \to \infty. \quad (3.8)$$

Thus a long-wave instability occurs only for $f(d) < 0$. This condition places an upper limit on the value of the bulk modulus $|G(\phi_0)|$ if an instability has to occur at $\phi = \phi_0$. We may determine the value of $G(\phi_0)$, or rather g_0 (cf. (2.1*g*)), by demanding the state of uniform fluidization to be marginally stable for a critical voidage of ϕ_c; this can be accomplished by selecting the value of g_0 via evaluating the condition $f(d) = 0$ at $\phi_0 = \phi_c$. Notice that g_0 can be determined uniquely from ϕ_c, but not vice versa.

To see this more clearly, consider the case of constant bulk modulus, G (i.e. $m_1 = 1$, $m_2 = 0$ in (2.1*g*)), and $\delta = 0$, upon which the condition $f(d) \leqslant 0$ becomes $g_0 \leqslant g_*(1-\phi_0)^2\phi_0^{2(n+1)}$, where g_* is a constant (Needham & Merkin 1986; for $\delta \neq 0$ see Göz 1993*b*). Choosing a value of g_0 between zero and a maximum value yields two critical voidage values, $0 < \phi_c^l < \phi_c^u < 1$, satisfying $f(d) = 0$; roughly speaking, one of these voidage values lies in the dense, the other in the dilute regime of fluidized beds. Incorporating a nonlinear particle pressure of the type (2.1*g*) merely shifts the lower endpoint from 0 to ϕ_{cp}. Thus, for a given $g_0 = g_0(\phi_c)$, ϕ_c representing either the lower or the upper critical voidage value, a uniformly fluidized state with a voidage of ϕ_0 will be linearly unstable only if $\phi_c^u > \phi_0 > \phi_c^l$. In practice, $\phi_c^l > \phi_{cp}$, so the value of g_0 is usually assumed to be larger than $g_0(\phi_{cp})$.†

In the following, we want to restrict our considerations to the dense regime in which there is a one-to-one relationship between $\phi_c^{(l)}$ and g_0, such that g_0 increases with ϕ_c; we will henceforth focus our attention on instabilities in a dense fluidized bed (i.e. ϕ_0 in the vicinity of ϕ_c^l) and drop the superindex '*l*'.

† We mention in passing that if the value of the bulk modulus respectively g_0 is 'too small', then $f(h)$ will also become negative so that $\mathrm{Re}(\sigma)$ tends to a positive constant as the longitudinal wavelength becomes very short ($\lambda \to \infty$). This can be avoided in principle by adding regularizing terms to the equations (Komatsu & Hayakawa 1993; Göz 1995*a*). This problem does not arise if we restrict the bulk moduli such that g_0 is larger than $g_0(\phi_{cp})$; so we will not consider the possibility of $f(h) < 0$, whose effects on the bifurcation behaviour were discussed by Göz (1992, 1993*b*).

	Air	Water
ρ_f (g cm^{-3})	0.0013	1
μ_f (g cm^{-1} s^{-1})	0.000181	0.0100556
g_0^{max}	229.1	0.0277
$g_0(\phi_{cp})$	57.4	0.00778
u_0 (cm s^{-1})	20.37	0.20
$F = u_0^2/(gr_p)$	28.2	0.00272
$R = \rho_s u_0 r_p/\mu_s^0$	0.101	0.00099

TABLE 1. Basic and deduced parameters used for the comparison of an air- and a water-fluidized bed. For both fluidized beds, $\rho_s = 2.2\,\mathrm{g\,cm^{-3}}$, $r_p = 0.015\,\mathrm{cm}$, $\mu_s^0 = 6.65\,\mathrm{g\,cm^{-1}\,s^{-1}}$, $\phi_0 = 0.43$ and $n = 3$, which yields $d = 2.85$ according to definition (3.7). The g_0-quantities are discussed in the text immediately after (3.8).

At this stage, it is useful to consider specific examples and we choose the two fluidized beds indicated in table 1. One column in this table gives the parameter values for a bed of glass beads of 300 μm diameter fluidized by air, while the other corresponds to the same bed fluidized by water. As we have not derived any expression for the particle-phase pressure in terms of the physical properties of the fluidized bed, we cannot determine the value of g_0, respectively ϕ_c, for each of these beds and are forced to treat it as a model parameter. In the numerical examples discussed here, we will consider the case of a constant bulk modulus and examine the fate of non-uniform solutions emerging from the loss of stability of uniformly fluidized beds having a voidage $\phi_0 = 0.43$. The quantity g_0^{max} indicated in table 1 refers to the value of the bulk modulus that would render the uniform state $\phi_0 = 0.43$ marginally stable. Thus, for any value of g_0 smaller than this value, the uniform state $\phi_0 = 0.43$ will be unstable. As noted earlier, for every assumed value of g_0, one can find the corresponding ϕ_c (in the dense regime) of the marginally stable uniform state. As we decrease g_0 from g_0^{max}, the value of ϕ_c decreases monotonically from 0.43 and attains the value of ϕ_{cp} when g_0 is equal to the value $g_0(\phi_{cp})$ shown in table 1.

When $\phi_0 > \phi_c$, the uniform state is linearly unstable for a range of longitudinal wavenumbers $0 < \lambda < \lambda_0$. At least in the vicinity of ϕ_c, both λ_0 and the maximum growth rate, $\mathrm{Re}(\sigma_m)$, which occurs at some intermediate wavenumber $\lambda_m \in (0, \lambda_0)$, increase as $(\phi_0 - \phi_c)$ increases; cf. table 2 and figure 1. Now, to illustrate how $(\phi_0 - \phi_c)$ affects the growth rate vs. longitudinal wavenumber curve, the natural approach would be to plot such curves for various values of ϕ_0 with a fixed value of ϕ_c (for example, see Anderson *et al.* 1995). We will adopt a slightly different approach where we will fix the value of ϕ_0 and vary ϕ_c, as it is more convenient for the present purpose. (As ϕ_0 changes, u_0 changes which in turn changes F, R, etc. and it becomes cumbersome to isolate the effect of $(\phi_0 - \phi_c)$ from those due to the other changes. In contrast, if we change ϕ_c while keeping ϕ_0 constant, we do not change F, R, etc. and change only $(\phi_0 - \phi_c)$.)

Accordingly, we assume that $\phi_0 = 0.43$ and consider several different values of ϕ_c, and calculate the value of the constant bulk modulus, $g_0(\phi_c)$, for every ϕ_c, see table 2. We then plot the dispersion curves (3.6) (with ω set to zero) for these parameters, see figure 1, and determine the maximum growth rates and the corresponding wavelengths. Note that figures 1(*a*) and 1(*b*) have been plotted in terms of dimensional quantities. This is necessary for our ensuing discussion of the correct scaling for the growth rate, as there exist no unique velocity and time scales for the problem. For the formal

Air-Fluidized Bed							
ϕ_c	$g_0(\phi_c)$	$-f(d)$	ω_0	λ_0	λ_m	$\mathrm{Re}(\sigma_m)$	$\mathrm{Re}(\sigma_m^*)$ (s^{-1})
0.422	202.7	0.93	2.681	0.0173	0.0108	5.06×10^{-4}	0.687
0.424	209.1	0.71	2.723	0.0149	0.0095	3.15×10^{-4}	0.427
0.426	215.6	0.48	2.765	0.0121	0.0079	1.57×10^{-4}	0.213
0.428	222.3	0.24	2.807	0.0085	0.0058	0.45×10^{-4}	0.061
Water-Fluidized Bed							
ϕ_c	$g_0(\phi_c)$	$-f(d)$	ω_0	λ_0	λ_m	$\mathrm{Re}(\sigma_m)$	$\mathrm{Re}(\sigma_m^*)$ (s^{-1})
0.422	0.02477	0.68	2.709	0.1169	0.0813	7.45×10^{-6}	9.94×10^{-5}
0.424	0.02548	0.51	2.744	0.1008	0.0704	4.27×10^{-6}	5.69×10^{-5}
0.426	0.02621	0.35	2.779	0.0819	0.0575	1.93×10^{-6}	2.58×10^{-5}
0.428	0.02696	0.17	2.814	0.0577	0.0406	0.49×10^{-6}	0.66×10^{-5}

TABLE 2. Primary instability in air- and water-fluidized beds. $\phi_0 = 0.43$. All quantities with the exception of $\mathrm{Re}(\sigma_m^*)$ are dimensionless. Further details on the two fluidized beds can be found in table 1. The quantity $g_0(\phi_c)$ is calculated assuming that the bulk modulus is independent of ϕ_0; see text immediately after (3.8).

calculations it is convenient to base these scales on the fluidization velocity u_0, and we have included the dimensionless maximum growth rates in table 2, but since u_0 is not a fixed quantity we have eventually to refer to dimensional growth rates.

Next, we get the wave velocities and wavelengths at the stability boundary by setting $\sigma = 0$ in (3.6):

$$\omega_0 = c + (c^2 + m - c)^{1/2}, \quad \lambda_0^2 = \frac{E(d - \omega_0)}{\tilde{J}(\omega_0 - h)}. \tag{3.9}$$

It is at these values where saturated one-dimensional travelling waves bifurcate from the uniform state†. In addition, we calculate $-f(d)$ through (3.7) as it can be viewed as a measure of the strength of the instability according to (3.8). From the values reported in table 2 it is clear that for given $(\phi_0 - \phi_c)$, the values of $f(d)$ for the two fluidized beds are of comparable magnitudes.

It is well-known that the maximum dimensional growth rates obtained for parameter values typical of gas-fluidized beds are considerably larger than those obtained for most liquid-fluidized beds (Anderson & Jackson 1968). Although casting the equations in a dimensionless form using the particle size, fluidization velocity and particle density as characteristic quantities (as we have done here) brings the dimensionless growth rates for the gas- and liquid-fluidized beds closer, they continue to differ by one or two orders of magnitude; see table 2. A proper scale for this maximum growth rate in terms of the system parameters has remained elusive so far. We will now deduce this scaling by examining the weakly unstable case in detail.

As mentioned above, $-f(d)$ measures the strength of the instability, so in the weakly unstable case we assume it to be small, $f(d) = -\epsilon$. Because the waves are long in this situation, we have to introduce $\lambda^2 = \epsilon\hat{\lambda}^2$, and have to scale σ appropriately. The eigenvalue deduced from (3.6) (with ω set to zero) through such a perturbation

† If $f(h) < 0$, then there is another solution $\omega_- = c - (f(c))^{1/2}$ to the determining equation $f(\omega) = 0$, cf. Göz (1993*b*).

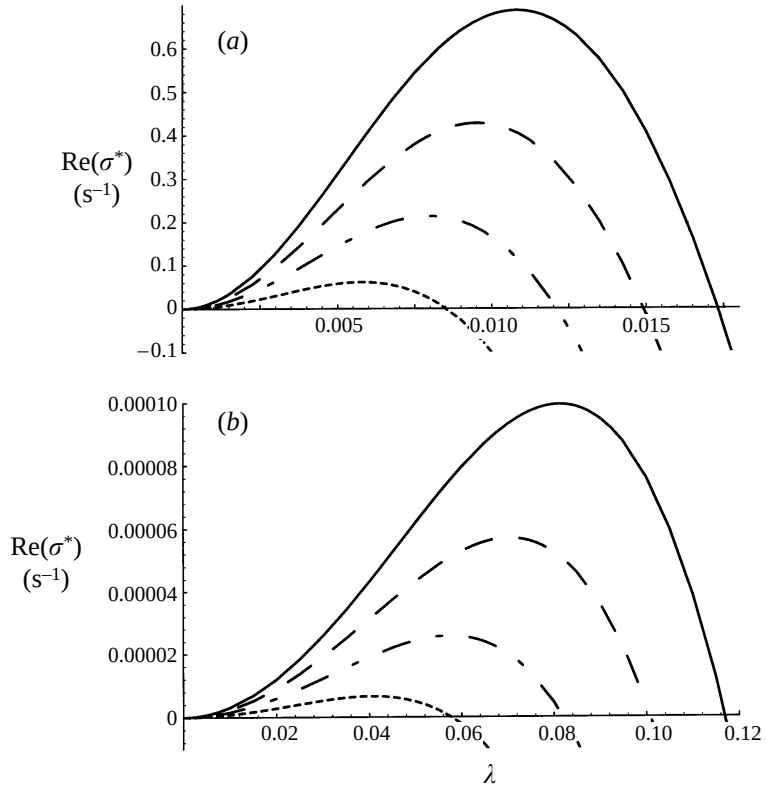

FIGURE 1. Dimensional primary growth rates $\mathrm{Re}\,(\sigma)$ vs. the longitudinal wavelength λ for various values of the bulk modulus resp. ϕ_c (cf. table 2). (*a*) Air-fluidized bed, (*b*) water-fluidized bed. The curves are for $\phi_c = 0.422$ (—), $\phi_c = 0.424$ (– – –), $\phi_c = 0.426$ (– - –), $\phi_c = 0.428$ (- - -). $\phi_0 = 0.43$ for all curves.

analysis becomes

$$\sigma = -\mathrm{i}d\hat{\lambda}\epsilon^{1/2} + \mathrm{i}\frac{\tilde{J}}{E}(d-h)\hat{\lambda}^3\epsilon^{3/2} + \frac{A}{E}\left[1 - 2\frac{\tilde{J}}{E}(d-c)(d-h)\hat{\lambda}^2\right]\hat{\lambda}^2\epsilon^2 + O(\epsilon^{5/2}).$$

The growth rate assumes its maximum

$$\mathrm{Re}\,\sigma_m = \frac{A}{8\tilde{J}(d-c)(d-h)}\epsilon^2 + O(\epsilon^3) \tag{3.10a}$$

at $\lambda_m^2 = \epsilon E/[4\tilde{J}(d-c)(d-h)] + O(\epsilon^2)$. Furthermore, the strength of the instability, $\epsilon = -f(d)$, can be expressed in terms of the distance from the stability boundary via $d - \omega_0 = \epsilon/[2(d-c)] + O(\epsilon^2)$. The scale for the growth rate should therefore be extracted by analysing the leading term on the right-hand side of (3.10*a*). From table 2 we know already that for small $(\phi_0 - \phi_c)$, the values of $f(d)$ are small and of comparable magnitudes for the two fluidized beds under consideration. The values of the quantity $(d-c)(d-h)$ appearing in (3.10*a*) are also very similar (8.120 and 7.044 for the air- and water-fluidized beds, respectively), so that the difference in the dimensionless growth rates of the two beds arises primarily as a result of $A/\tilde{J}$ in (3.10*a*). As

$$\frac{A}{\tilde{J}} = \frac{\phi_0 + \delta(1-\phi_0)}{\phi_0(1+\kappa) + O(v)}(1-\phi_0)R, \tag{3.10b}$$

with a prefactor of comparable magnitude (0.57 and 0.91 for the air- and water-fluidized beds, respectively), we conclude that the magnitude of the dimensionless primary growth rate is proportional to the Reynolds number, as long as ϵ is small. The dimensional growth rate is then proportional to ϵ^2 and $u_0 R/r_p = \rho_s u_0^2/\mu_s^0$ (with a proportionality factor of 8.8×10^{-3} and 16×10^{-3} for the air- and water-fluidized beds, respectively), so that *for given particle density and viscosity the scale for the growth rate is set by the square of the fluidization velocity*.

In the calculations summarized in table 2, we have assumed identical values for ρ_s and μ_s^0 for both water- and air-fluidized beds. Therefore, the dimensional growth rate in these two beds at comparable ϵ should differ by about 10^4, as the velocities differ by a factor of 10^2. We may also bring the Froude number into play by writing $u_0 R/r_p = F\rho_s g r_p/\mu_s^0$; although this involves an additional dependency on the particle radius, the values quoted in the tables indicate the simple criterion of small (large) growth rates for $F \ll 1$ ($F \gg 1$). Furthermore, these considerations suggest a natural time scale of $\mu_s^0/(\rho_s u_0^2)$ and a length scale of $\mu_s^0/(\rho_s u_0)$, possibly weighed with $1/f^2(d)$ and $1/(-f(d))^{1/2}$, respectively; however, we shall not pursue this further here.

Rewriting (2.4) in the form $u_0 = (2g/9)\rho_s \phi_0^{n+1} r_p^2 (1-\delta)/\mu_f$ reveals the influence of δ and μ_f with all other parameters fixed. These particular parameters enter in two ways: implicitly through the just mentioned constitutive relation, and explicitly through the terms in (2.1*d*) accounting for the inertia and viscosity of the fluid phase. They make their greatest impact through u_0, which is related to balancing drag and buoyancy with gravity; neglecting the terms proportional to δ and ν in (2.1*d*) leads to $C = \tilde{H} = 0$ in the dispersion relation (3.6), but this has been found to play a minor role.

To conclude this subsection, we note that (3.6) can be evaluated in any travelling wave frame. Nevertheless, it is worthwhile to identify specific travelling wave frames which we will employ in the analyses described in the next subsections. In §3.3, we will consider time-dependent, small-amplitude, one-dimensional waves of arbitrary λ which have just started to grow because of an instability of the uniform state, and examine the initial growth rates of transverse perturbations superimposed on them. Here, a natural choice of ω will be the propagation velocity of the corresponding linear one-dimensional wave. For example, if we consider the fastest growing one-dimensional wave (corresponding to $\lambda = \lambda_m$), then we will choose ω to be the propagation speed of this wave, $\omega_m = \mathrm{Im}(\sigma_m)/\lambda_m$. Then, in this moving frame, the eigenvalue for the one-dimensional wave becomes real, $\sigma = \mathrm{Re}(\sigma_m)$.

In §4, we will consider fully developed one-dimensional travelling waves of small amplitude, which are possible only in the vicinity of the Hopf bifurcation point, (λ_0, ω_0), and examine their stability to transverse perturbations. One can expect the velocities and longitudinal wavelengths of these fully developed one-dimensional waves to differ only slightly from those of a linear wave at $\lambda = \lambda_0$. Therefore, to leading order, we can set $\lambda \approx \lambda_0$ and $\omega \approx \omega_0$, which is the propagation velocity of the linear wave at $\lambda = \lambda_0$, cf. (3.9).

3.2. *Two-dimensional perturbations of one-dimensional waves*

We know from many previous investigations that the uniform state is most unstable to vertical perturbations, and that this leads to plane travelling waves (Needham & Merkin 1986; Göz 1993*b*). But until recently it has been quite unclear whether (and why) the two-fluid model allows for a secondary instability, where these waves become unstable to transverse perturbations (Hernández & Jiménez 1991; Göz 1995*c*, Anderson *et al.* 1995; Glasser *et al.* 1996, 1997). We extend these works in that

we investigate analytically the full two-fluid model with respect to two aspects: we consider the behaviour of two-dimensional modes during the growth of the most unstable one-dimensional mode, and we calculate the transverse stability of a small-amplitude saturated one-dimensional wave train. This will lead to a thorough comparison of gas- and liquid-fluidized beds in the weakly nonlinear regime near the onset of the primary instability. In order to clarify our notation, we note that ϕ_0 is the voidage of the uniformly fluidized state, $\phi_0 + \phi_1(z,t)$ is the vertically travelling one-dimensional wave and $\phi_0 + \phi_1(z,t) + \phi(y,z,t)$ is the voidage profile including the two-dimensional disturbance. The other variables are represented in a similar manner.

We linearize the equations (2.7), (2.8), (2.10) and (2.11) about a one-dimensional solution of the type described above, separate the dependence of the perturbation on the horizontal coordinate by an exponential factor,

$$(\phi, p, v_z, v_y, u_z, u_y) = (\psi, q, u, w, \eta, \rho)\mathrm{e}^{\mathrm{i}ky}, \tag{3.11}$$

and keep only those terms which are linear in the one-dimensional solution according to (3.2). This leaves us with the following equation for the voidage:

$$FK\psi = r_\psi = O(\phi_1), \tag{3.12a}$$

with the modified linear part

$$\begin{aligned} K\psi = {} & A\ddot{\psi} + 2(C - A\omega)\dot{\psi}' + (A\omega^2 - 2C\omega + C - M)\psi'' + Mk^2\psi \\ & + (E + \tilde{J}k^2)\dot{\psi} + [D - E\omega + (\tilde{H} - \tilde{J}\omega)k^2]\psi' - \tilde{J}\dot{\psi}'' + (\tilde{J}\omega - \tilde{H})\psi'''. \end{aligned} \tag{3.12b}$$

and the right-hand side r_ψ given in Appendix B. We will set up similar equations for the other variables (q, u, w, η, ρ) as well ((3.13)–(3.15) below). We will then represent the variables $(\psi, q, u, \ldots)$ in terms of mixed modes and a transverse-only mode (according to (3.18) below) and derive expressions for amplitudes of each of these modes. This will then prepare us for the analysis of the growth rate of two-dimensional perturbations presented in §§3.3 and 4.

Now, the other variables follow from the equations

$$\begin{aligned} (1 - \phi_0)(q'' - k^2 q) = {} & -F\ddot{\psi} + 2F\omega\dot{\psi}' + k^2 G_0\psi - (G_0 + F\omega^2)\psi'' + a_1\psi' \\ & -(EF + c_1k^2)\dot{\psi} + c_1\dot{\psi}'' - (c_1\omega + \alpha_1 FH)\psi''' + r_q, \end{aligned} \tag{3.13}$$

with $r_q = O(\phi_1)$ as given in Appendix B, and

$$\begin{aligned} & F(1 - \phi_0)(\dot{u} - \omega u') - \mu u'' + \mu k^2 u - B_0(\eta - u) - v_1\eta'' + v_1 k^2\eta \\ & \qquad = b_1\psi - G_0\psi' + \mu_1\dot{\psi}' - \mu_2\psi'' - (1 - \phi_0)q' + r_u, \end{aligned} \tag{3.14a}$$

$$\begin{aligned} & F(1 - \phi_0)(\dot{w} - \omega w') - \mu w'' + \mu k^2 w - B_0(\rho - w) - v_1\rho'' + v_1 k^2\rho \\ & \qquad = \mathrm{i}k\left[-G_0\psi + \mu_1\dot{\psi} - \mu_2\psi' - (1 - \phi_0)q\right] + r_w, \end{aligned} \tag{3.14b}$$

$$\begin{aligned} & F\delta\phi_0[\dot{\eta} + (1 - \omega)\eta'] - v_2\eta'' + v_2 k^2\eta + B_0(\eta - u) \\ & \qquad = -b_\delta\psi - \frac{v_2\bar{\kappa}}{\phi_0}[\dot{\psi} + (1 - \omega)\psi']' - \phi_0 q' + r_\eta, \end{aligned} \tag{3.15a}$$

$$\begin{aligned} & F\delta\phi_0[\dot{\rho} + (1 - \omega)\rho'] - v_2\rho'' + v_2 k^2\rho + B_0(\rho - w) \\ & \qquad = -\mathrm{i}k\left[\frac{v_2\bar{\kappa}}{\phi_0}\{\dot{\psi} + (1 - \omega)\psi'\} + \phi_0 q\right] + r_\rho. \end{aligned} \tag{3.15b}$$

The expressions for the $r_* = O(\phi_1)$ as well as the constants a_i, $i = 1, \ldots$, appearing here and below will be given in Appendix B. Instead of evaluating (3.14a, b) and

(3.15*a*, *b*), however, it is sometimes more convenient to use the linearizations of (2.6*a*, *b*), leading to

$$(1-\phi_0)(\mathrm{i}kw+u')=\dot{\psi}-\omega\psi'+r_1, \tag{3.16}$$

$$\phi_0(\mathrm{i}k\rho+\eta')=-\dot{\psi}-(1-\omega)\psi'+r_2, \tag{3.17}$$

because with these two relations the transverse velocity components w and ρ can be eliminated easily from the leading-order contributions to r_ψ (cf. Appendix B. Here we use (3.16), (3.17) instead of (3.14), (3.15*b*); for the asymptotic analysis in §4 we shall use them instead of (3.14), (3.15*a*)). To proceed we now break down the above expressions into their basic harmonic components.

As in Göz (1995*c*), we assume that the perturbation has the same wavelength and travels at the same wave speed as the primary wave. Neglecting contributions from higher harmonics, similar to the one-dimensional case, but including pure transverse perturbations, the two-dimensional perturbations can be decomposed as

$$(\psi,q,u,\ldots)=(\psi,q,u,\ldots)_+\,\mathrm{e}^{\mathrm{i}\lambda z}+(\psi,q,u,\ldots)_-\,\mathrm{e}^{-\mathrm{i}\lambda z}+(\psi,q,u,\ldots)_0+\text{h.h.}, \tag{3.18}$$

where the first two terms on the right-hand side denote the mixed modes, the third term is the pure transverse mode and h.h. means higher harmonics. Consequently, we should also neglect higher-harmonic terms arising from the quasi-linear terms in r_ψ. Inserting this into (3.12) yields the three equations

$$A\ddot{\psi}_+ + a_2\dot{\psi}_+ + a_3\psi_+ = F^{-1}\,r_{\psi|_{\exp(\mathrm{i}\lambda z)}} = F^{-1}\,r_+, \tag{3.19a}$$

$$A\ddot{\psi}_- + \bar{a}_2\dot{\psi}_- + \bar{a}_3\psi_- = F^{-1}\,r_{\psi|_{\exp(-\mathrm{i}\lambda z)}} = F^{-1}\,r_-, \tag{3.19b}$$

$$A\ddot{\psi}_0 + (E+\tilde{J}k^2)\dot{\psi}_0 + Mk^2\psi_0 = F^{-1}\,r_{\psi|_{e0}} = F^{-1}\,r_0, \tag{3.19c}$$

where (cf. Appendix B)

$$r_+ = \phi_+[\gamma_1\psi_0+\gamma_2\dot{\psi}_0+\gamma_3\eta_0+\gamma_4u_0-k^2q_0+O(\phi_+,\phi_-)], \tag{3.20a}$$

$$r_- = r_+(\phi_+\to\phi_-,\ \gamma_i\to\bar{\gamma}_i), \tag{3.20b}$$

$$\begin{aligned} r_0 = {}& \phi_+[\mathrm{i}\lambda(\gamma_5\eta_- - \gamma_6u_-)+\gamma_7\dot{\psi}_- + \bar{\gamma}_8\psi_- - k^2q_- + O(\phi_-)] \\ & +\phi_-[-\mathrm{i}\lambda(\gamma_5\eta_+ - \gamma_6u_+)+\gamma_7\dot{\psi}_+ + \gamma_8\psi_+ - k^2q_+ + O(\phi_+)]. \end{aligned} \tag{3.20c}$$

The structure of these equations reveals clearly how the different modes interact with each other. The pure transverse mode $(\psi,q,u,\ldots)_0$ strengthens or weakens the pair of 'mixed modes' $(\psi,q,u,\ldots)_\pm$, and vice versa, by interaction with the primary mode $\phi_\pm$. It is also seen that the longitudinal self-interaction becomes effective in the higher-order terms only.

Moreover, (3.13) gives

$$q_+ = \frac{F}{(1-\phi_0)(\lambda^2+k^2)}\ddot{\psi}_+ + a_4\dot{\psi}_+ + a_5\psi_+ + O(\phi_+), \tag{3.21a}$$

$$q_- = \frac{F}{(1-\phi_0)(\lambda^2+k^2)}\ddot{\psi}_- + \bar{a}_4\dot{\psi}_- + \bar{a}_5\psi_- + O(\phi_-), \tag{3.21b}$$

$$(1-\phi_0)k^2\,q_0 = F\ddot{\psi}_0 + (EF+c_1k^2)\dot{\psi}_0 - G_0k^2\psi_0 - r_q^0, \tag{3.21c}$$

while (3.14) and (3.15) lead to

$$F(1-\phi_0)\dot{u}_+ + a_{61}u_+ - a_{62}\eta_+ = \mathrm{i}\lambda\mu_1\dot{\psi}_+ + a_7\psi_+ - \mathrm{i}\lambda(1-\phi_0)q_+ + O(\phi_+), \tag{3.22a}$$

$$\begin{aligned} F(1-\phi_0)\dot{w}_+ + a_{61}w_+ - a_{62}\rho_+ = {}& \mathrm{i}k\,[\mu_1\dot{\psi}_+ - (G_0+\mathrm{i}\lambda\mu_2)\psi_+] \\ & -\mathrm{i}k(1-\phi_0)q_+ + O(\phi_+), \end{aligned} \tag{3.22b}$$

$$F\delta\phi_0\dot{\eta}_+ + a_8\eta_+ - B_0u_+ = -\mathrm{i}\lambda v_2\frac{\bar{\kappa}}{\phi_0}\dot{\psi}_+ - a_9\psi_+ - \mathrm{i}\lambda\phi_0 q_+ + O(\phi_+), \tag{3.23a}$$

$$F\delta\phi_0\dot{\rho}_+ + a_8\rho_+ - B_0w_+ = -\mathrm{i}k\left[v_2\frac{\bar{\kappa}}{\phi_0}\{\dot{\psi}_+ + \mathrm{i}\lambda(1-\omega)\psi_+\} + \phi_0 q_+\right] + O(\phi_+), \tag{3.23b}$$

corresponding equations for u_-, w_-, η_- and ρ_-, and

$$F(1-\phi_0)\dot{u}_0 + (\mu k^2 + B_0)u_0 - (B_0 - v_1k^2)\eta_0 = b_1\psi_0 + r_u^0 + O(\phi_+\phi_-), \tag{3.24a}$$

$$F(1-\phi_0)\dot{w}_0 + (\mu k^2 + B_0)w_0 - (B_0 - v_1k^2)\rho_0 = \mathrm{i}k\,[\mu_1\dot{\psi}_0 - G_0\psi_0 - (1-\phi_0)q_0] + r_w^0 + O(\phi_+\phi_-), \tag{3.24b}$$

$$F\delta\phi_0\dot{\eta}_0 + (v_2k^2 + B_0)\eta_0 - B_0u_0 = -b_\delta\psi_0 + r_\eta^0 + O(\phi_+\phi_-), \tag{3.25a}$$

$$F\delta\phi_0\dot{\rho}_0 + (v_2k^2 + B_0)\rho_0 - B_0w_0 = -\mathrm{i}k\left(v_2\frac{\bar{\kappa}}{\phi_0}\dot{\psi}_0 + \phi_0 q_0\right) + r_\rho^0 + O(\phi_+\phi_-). \tag{3.25b}$$

The higher-order terms like $r_u^0 = O(\phi_+, \phi_-)$ follow from taking the average of r_u with respect to z. Note that except in the voidage equations (3.19), we have included higher-order terms in the averaged equations only (those with the zero index denoting the pure transverse modes), as it will turn out that we only need these. This means that *for relating pressure and velocity of the mixed modes to the voidage, the relationships stemming from the linearization at the uniform state are sufficient, whereas we need to look at higher-order contributions to determine the pure transverse modes.* Evaluating (3.16) and (3.17) leads to

$$(1-\phi_0)(\mathrm{i}kw_+ + \mathrm{i}\lambda u_+) = \dot{\psi}_+ - \mathrm{i}\lambda\omega\psi_+ + \mathrm{i}k\phi_+w_0 + \mathrm{i}\lambda(\phi_+u_0 + v_{1+}\psi_0), \tag{3.26a}$$

$$(1-\phi_0)\mathrm{i}kw_0 = \dot{\psi}_0 + \mathrm{i}k(\phi_+w_- + \phi_-w_+)\,; \tag{3.26b}$$

$$\phi_0(\mathrm{i}k\rho_+ + \mathrm{i}\lambda\eta_+) = -\dot{\psi}_+ - \mathrm{i}\lambda(1-\omega)\psi_+ - \mathrm{i}k\phi_+\rho_0 - \mathrm{i}\lambda(\phi_+\eta_0 + u_{1+}\psi_0)\,, \tag{3.27a}$$

$$\phi_0\mathrm{i}k\rho_0 = -\dot{\psi}_0 - \mathrm{i}k(\phi_+\rho_- + \phi_-\rho_+)\,. \tag{3.27b}$$

As noted earlier at the end of §3.2, there are two ways to proceed. First, we can look at the evolution of the two-dimensional modes as a primary wave of arbitrary longitudinal wavenumber λ grows. Owing to the nature of the above approximation, this will be limited to small amplitudes of the one-dimensional wave and, hence, to short times. Then we might even neglect the time-dependence of the one-dimensional wave and approximate the initial development of the perturbation modes by an eigenvalue problem. (Another way to view this approach is to say that we analyse the stability of the growing one-dimensional wave via a quasi-steady-state approximation, where we fix its time-dependent amplitude at various stages.) This will be carried out in the next subsection, where we will study the dependence of the initial (i.e. for small time intervals) two-dimensional growth rates on the amplitude of the growing one-dimensional wave and the lateral wavenumber for the two fluidized beds under consideration. Second, we can use the above equations to investigate the stability of a fully developed small-amplitude one-dimensional travelling wave. In this case we have to put $\sigma = 0$ everywhere, which leads to a singularity for small transverse wavenumbers. This singularity indicates that the transverse variables act on a scale of the order of the square root of the one-dimensional amplitude; the appropriate

rescaling performed in §4 leads to the proof of the presence of a long-wave secondary instability.

3.3. *Initial secondary growth rates*

In principle, equations (3.19)–(3.25) constitute the dynamical system controlling the initial growth of one- and two-dimensional modes. It is far too large, however, and should be simplified further, preferably to a system like (3.19) but for the voidage variables only by eliminating (most of) the other variables. To achieve this, we employ the following trick. From (3.19*a*) we observe that to leading order $\ddot{\psi}_+$ can be expressed as a linear function of ψ_+ and $\dot{\psi}_+$. Insertion into (3.21*a*) gives q_+ in terms of ψ_+ and $\dot{\psi}_+$, plus higher-order corrections which we may neglect. Then (3.22*a*) and (3.23*a*) suggest that u_+ and η_+ may also be expressed in first approximation as linear combinations of the 'basis functions' ψ_+ and $\dot{\psi}_+$, thereby neglecting damped homogeneous solutions to these equations. Therefore we propose

$$(q_+, u_+, \eta_+) = (c_q^+, c_u^+, c_\eta^+)\,\dot{\psi}_+ + (\tilde{c}_q^+, \tilde{c}_u^+, \tilde{c}_\eta^+)\,\psi_+ + O(\phi_\pm)\,, \tag{3.28}$$

and similarly for the variables with the minus or zero index†. The constant coefficients can be found in Appendix C. The results are then used to remove the pressure and velocity variables from (3.20), so that we finally end up with three second-order non-autonomous but linear equations for the voidage variables:

$$A\ddot{\psi}_+ + a_2\dot{\psi}_+ + a_3\psi_+ = \theta_1\phi_+\dot{\psi}_0 + \theta_2\phi_+\psi_0\,, \tag{3.29a}$$

$$A\ddot{\psi}_- + \bar{a}_2\dot{\psi}_- + \bar{a}_3\psi_- = \bar{\theta}_1\phi_-\dot{\psi}_0 + \bar{\theta}_2\phi_-\psi_0\,, \tag{3.29b}$$

$$A\ddot{\psi}_0 + (E + \tilde{J}k^2)\dot{\psi}_0 + Mk^2\psi_0 = \theta_3\phi_-\dot{\psi}_+ + \bar{\theta}_3\phi_+\dot{\psi}_- + \theta_4\phi_-\psi_+ + \bar{\theta}_4\phi_+\psi_-, \tag{3.29c}$$

where higher-order terms (quadratic in $\phi_\pm$ or stemming from higher harmonics) have been omitted. The constants θ_i are given in Appendix C.

Let us now consider a one-dimensional travelling wave corresponding to the fastest growing mode (i.e. $\lambda = \lambda_m$). A fully developed travelling wave of this wavenumber will, in general, not have a small amplitude, so we must consider a growing one-dimensional wave at a stage when its amplitude is small (if we wish to use (3.29)). Therefore we will set $\phi_+ = v_p \exp(\sigma t)$ as in (3.3) where v_p denotes the current amplitude (the current time being taken to be $t = 0$ without loss of generality) and σ is the maximum growth rate of the primary instability (=Re(σ_m), cf. table 2). Although (3.29) can now be solved numerically, we will restrict our attention to the simpler problem of estimating the initial growth rate of the two-dimensional perturbation by simply setting ϕ in these equations equal to v_p. This approximation reduces (3.29)

† We remark that it is indeed acceptable to neglect the contributions from the homogeneous solutions to (3.22*a*) and (3.23*a*) (the $\pm$ velocity modes), because these are strongly damped. More precisely, their decay rate is of the order of $-\lambda_0^2$, and we consider λ_0 as being of order one. This is less clear with regard to the homogeneous solutions of (3.24*a*), (3.25*a*) as the decay rate of these zero-index modes, representing vertical velocity components with transverse-only structure, is of the order of $-k^2$, which may be small. We shall see in the next section that the modes with small transverse wavenumber drive the secondary instability and thereby the presence of a transverse contribution to the vertical velocity may play a role. Although discarding this pure velocity perturbation mode in (3.29) can be somewhat misleading, the essential features of the secondary modes can already be detected by ignoring possibly amplifying terms like $\phi_+ u_0^0 \exp(\sigma_0 t)$ in (3.29*a*). Here, $\sigma_0 \sim -k^2$, while u_0^0 represents an initial perturbation of the vertical (fluid) velocity in the horizontal direction; hence, leaving out such terms amounts to disallowing the corresponding perturbations. In order to get a relation between u_0^0 and the voidage modes $\psi_{\pm,0}$ one has to consider higher-order terms; we spare us and the reader this here but shall have to address it in the rescaled analysis of the next section.

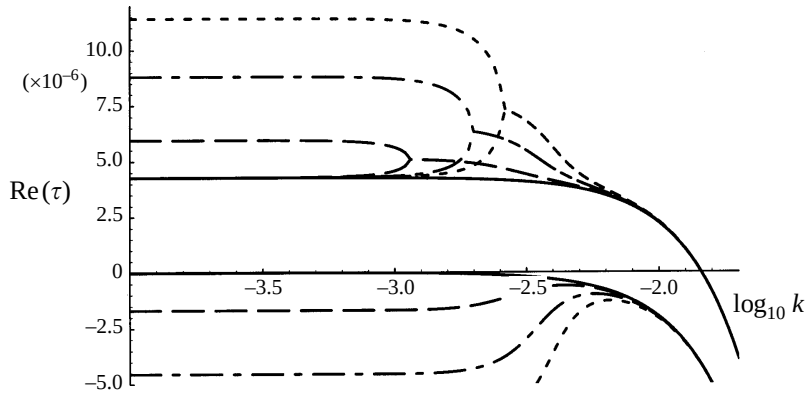

FIGURE 2. Dimensionless initial secondary growth rates according to the approximation (3.29) for a water-fluidized bed with $\phi_c = 0.424$ (see tables 1 and 2). The values of v_p are 0 (—), 7×10^{-7} (– – –), 1.4×10^{-6} (– - –), 2×10^{-6} (- - -).

to an eigenvalue problem and enables us to compare the initial growth rates of the primary and secondary disturbances. Strictly speaking, the rate of amplification of disturbances calculated through such an eigenvalue problem may have no relevance to the long-time behaviour (Wang, Jackson & Sundaresan 1996). Nevertheless it does serve two useful purposes for the present study. First, it reveals that the initial growth rate of the secondary instability is affected by the amplitude of the primary one-dimensional wave in a more profound manner in the case of a liquid-fluidized bed than in the case of a gas-fluidized bed. Secondly, it exposes the occurrence of a singularity at $k = 0$ in the case of fully developed (i.e. $\sigma = 0$) small-amplitude waves which occur in the vicinity of λ_0 and points to the need for a rescaled analysis.

The outcome of such an eigenvalue calculation is illustrated in figure 2 for the water-fluidized bed in table 1, where ϕ_c is taken to be 0.424 (see first row in table 2 under water-fluidized bed). For various assumed values of one-dimensional amplitude v_p and transverse wavenumber k, we have determined the six eigenvalues by solving (3.29). The real parts of the two leading eigenvalues are plotted in figure 2 as a function of k, for several different values of v_p; also shown in this figure is the next largest eigenvalue, which is real and negative for all k, and decreases with increasing v_p. For $v_p = 0$, the two leading eigenvalues appear as a complex-conjugate pair for all values of k, and their real part is shown in figure 2 as a solid line. The mixed modes represented by these eigenvalues are stable for large values of k, but become unstable as k is decreased sufficiently. As k is decreased further, the real part of the eigenvalues becomes virtually independent of k. The growth rate in this plateau region is virtually the same as that of the primary instability away from the uniform state. For non-zero values of v_p, the two leading eigenvalues appear as a complex-conjugate pair for large k values; however, as k is decreased they split into two real eigenvalues. It is clear from figure 2 that this splitting occurs at a higher and higher k value as v_p is increased. As k is decreased, one of the real eigenvalues decreases towards the plateau corresponding to $v_p = 0$, while the other eigenvalue increases towards a different plateau. The growth rate in this latter plateau increases as v_p increases, so the secondary mode corresponding to this eigenvalue grows much faster than the primary wave once the latter has reached an amplitude of the order of 10^{-6}.

Repeating this analysis for various values of ϕ_c revealed that the stronger the primary instability (i.e. the larger the magnitude of $\phi_0 - \phi_c$ resp. the smaller g_0) is,

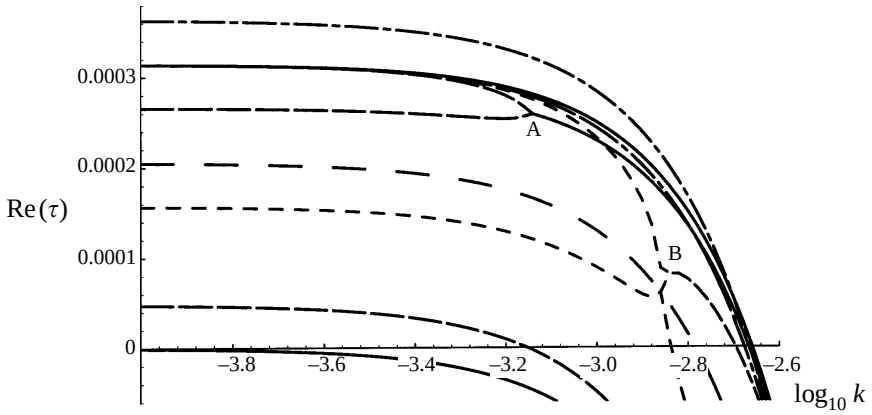

FIGURE 3. Dimensionless initial secondary growth rates according to the approximation (3.29) for an air-fluidized bed with $\phi_c = 0.424$ (see tables 1 and 2). The values of v_p are 0 (—), 8×10^{-4} (– – –), 1.5×10^{-3} (- - -), 2.5×10^{-2} (– – –), 5×10^{-2} (– - –).

the larger is the order of magnitude of v_p at which the secondary mode grows much faster than the primary mode.

A similar analysis for the case of a gas-fluidized bed is illustrated in figure 3 for the same ϕ_c of 0.424 (see table 2). The solid lines in figure 3 indicate the real part of the dominant complex-conjugate eigenvalue pair and the next largest eigenvalue (which happens to be real and corresponds to a transverse mode) for the case $v_p = 0$. As in the case of liquid-fluidized beds, the growth rate of the dominant eigenvalue is negative for large k, turns positive as k is decreased and becomes independent of k for sufficiently small k. Once again, for non-zero values of v_p, the two dominant eigenvalues appear as a complex conjugate pair for large k, and split into two real eigenvalues as k is decreased (e.g. see point A in figure 3). As k is decreased further, one of these two real eigenvalues increases towards the plateau corresponding to $v_p = 0$, while the other real eigenvalue decreases towards a different plateau. Simultaneously, the next largest eigenvalue increases as well. These are clearly seen in the curves corresponding to $v_p = 0.0008$. As the value of v_p is increased further (to 0.0015), the second and third real eigenvalue branches collide (as illustrated by point B in figure 3) and become a complex-conjugate pair for small k values. Focusing on this complex-conjugate pair at small k values, one finds that its growth rate continues to increase as v_p is increased. When $v_p = 0.06$, these secondary modes grow much faster than the primary wave. We have repeated this analysis for different values of ϕ_c and found the same trend as in the case of water-fluidized beds, i.e. as $(\phi_0 - \phi_c)$ increases, both the maximum growth rate of the primary instability and the typical value of v_p needed for the secondary mode to overwhelm the primary mode increase.

Comparing figures 2 and 3, it is apparent that the order of magnitude values of v_p at which the primary wave has an appreciable effect on the growth of the secondary modes are vastly different for the gas- and liquid-fluidized beds under consideration. This effect can also be worked out analytically. The six eigenvalues of (3.29) with constant $\phi_\pm$ $(= v_p)$ can be represented as a power series in v_p^2; for $v_p = 0$, the dominant eigenvalue belongs to the mixed modes, is a complex $O(k^2)$ perturbation of σ (primary

instability) and is given by the solution with positive real part of

$$A\tau_0^2 + a_2\tau_0 + a_3 = 0, \quad \text{i.e.} \quad \tau_0 = \sigma - O(k^2). \tag{3.30}$$

The other solution of (3.30) has negative real part. (Note that (3.30) follows from (3.29*a*) with $\phi_+ = v_p = 0$.) The complex-conjugate eigenvalues of these two are obtained as solutions of the equation with complex-conjugate coefficients that follows from (3.29*b*) with $\phi_- = v_p = 0$. The remaining two eigenvalues follow in the same way from (3.29*c*), hence are real (and belong to transverse modes); one is of order $-k^2$, the other is strongly negative. The expansion for the dominant eigenvalue in terms of v_p starts as

$$\tau = \tau_0 + \tau_2 v_p^2 + \tau_4 v_p^4 + O(v_p^6), \ \tau_2 = \frac{(\theta_1\tau_0 + \theta_2)(\theta_3\tau_0 + \theta_4)}{(2A\tau_0 + a_2)[A\tau_0^2 + (E + \tilde{J}k^2)\tau_0 + Mk^2]}, \tag{3.31}$$

and similarly for the complex-conjugate eigenvalue (the expression for τ_4 is too lengthy to be presented here but can easily be calculated with *Mathematica*). This approximation is valid as long as the contribution from the v_p^2 term is much smaller than τ_0; since this applies to both the real and imaginary parts of τ, the expansion will certainly fail when the split of the complex-conjugate eigenvalues into a pair of real eigenvalues occurs. Defining a critical v_p, v_p^c, for which $|\mathrm{Re}(\tau_2)|(v_p^c)^2 \sim |\mathrm{Re}(\tau_0)|$, we find that for the water-fluidized bed $v_p^c \sim O(10^{-6})$ to $O(10^{-4})$ depending on the choice of ϕ_c, while for the air-fluidized bed $v_p^c \sim O(10^{-3})$ to $O(10^{-1})$. These are comparable to the values found numerically (figures 2 and 3). (As figure 3 reveals that in the case of the air-fluidized bed one of the transverse modes (tm) is growing instead of the mixed mode and since the eigenvalue of the transverse mode starts with $\tau_0^{tm} = O(-k^2)$ as $k \to 0$, it is more reasonable to compare in this case τ_4^{tm} with τ_2^{tm} to estimate v_p^c. We simply note that this leads to the same estimate for v_p^c as noted above for the air-fluidized bed.)

Although the approximation (3.29) breaks down for much smaller one-dimensional amplitudes in the case of water-fluidized beds than air-fluidized beds, it does not mean that the approximation also becomes invalid earlier *in time*; in fact the opposite is true, because the primary waves grow so much faster in the air-fluidized bed and thus reach the critical amplitude in shorter time. We shall discuss this point further in §5 after finishing the rescaled stability analysis of a fully developed small-amplitude one-dimensional wavetrain.

In the derivation of (3.29) and the subsequent analysis described in this section, we have treated the vertical wavenumber, λ, as arbitrary. The amplitude of a fully developed one-dimensional wave corresponding to the chosen value of λ may be large, thereby rendering the approximation leading to (3.29) invalid. The requirement of a small-amplitude one-dimensional wave, coupled with our desire to leave λ arbitrary, led to time-dependent $\phi_\pm$ on the right-hand side of (3.29). We then made a gross simplification by neglecting the time-dependence of $\phi_\pm$ to extract an eigenvalue problem. This last simplification can be eliminated altogether if we insist that the one-dimensional wavetrain be fully developed. If we demand this, the vertical wavenumber can no longer be left arbitrary. Fully developed, small amplitude one-dimensional wavetrains can be obtained only in the vicinity of vertical wavenumber λ_0 (and corresponding wave velocity ω_0) satisfying (3.10). When we do examine the consequences of such fully developed, small amplitude one-dimensional wavetrains on the growth rates of secondary modes, a need for re-scaling the problem surfaces. This can be seen by putting $\sigma = 0$ not only in the exponential factor on the right-hand

side of (3.29) but also in the coefficients θ_i, and examining the outcome on (3.30) and (3.31). Then $\tau_0 = -O(k^2)$, so that

$$\tau_2 \sim \frac{(\theta_2\theta_4)^0}{a_2^0 k^2} + O(1), \qquad k^2 \ll 1, \tag{3.32}$$

because $\theta_{1,2} \sim 1/k^2$ while $\theta_{3,4} \sim k^2$ as $k \to 0$; the superscript zero means evaluation at $k = 0$. The singularity in (3.32) signals that for long-wave perturbations of fully-developed one-dimensional waves, (3.31) becomes invalid in the sense that we cannot consider v_p being small and k a quantity of order one; instead we have to relate the two. How this has to be done can be readily inferred from (3.31), (3.32): the perturbation term $\sim v_p^2/k^2$ becomes of the same order as the leading-order term $\sim k^2$ if $k^2 \sim v_p$; correspondingly the eigenvalue scales then as $\tau \sim v_p$. It turns out that this procedure involves a rescaling of other variables too, so that we have to retreat one step from (3.29) and work with the equations (3.19)–(3.27). The details of the rescaled analysis will be presented in the next section.

4. Asymptotic analysis

We now consider the stability of a fully developed small-amplitude one-dimensional wavetrain by analysing the equations (3.19)–(3.27), together with (3.3)–(3.5), for $\sigma = 0$ and $\phi_+ = \phi_- = \epsilon$. We will first describe the necessary rescaling and then derive a dispersion relation, (4.13), for the eigenvalues of the two-dimensional perturbations. We will then describe how the four eigenvalues which can be obtained from the dispersion relation vary with the transverse wavenumber for typical air- and water-fluidized beds. It is sufficient to approximate ω and λ by ω_0 and λ_0 characterizing the onset of the one-dimensional periodic solutions (see (3.9)), since the deviations are of order ϵ^2 and will not enter the calculations. In addition, we may assume $\psi_+ = \tilde{\psi}_+ \exp(\tau t)$, and similarly for the other variables, with the eigenvalue τ determining the stability of the one-dimensional wave to two-dimensional perturbations of the same longitudinal wavelength and velocity. Hence (3.19*a*) becomes

$$F(A\tau^2 + a_2\tau + a_3)\tilde{\psi}_+ = \epsilon[(\gamma_1 + \tau\gamma_2)\tilde{\psi}_0 + \gamma_3\tilde{\eta}_0 + \gamma_4\tilde{u}_0 - k^2\tilde{q}_0] + O(\epsilon^2), \tag{4.1}$$

where now $a_3 \sim k^2$ due to (3.9), cf. (B 1). It is easily seen that $\mathrm{Re}(\tau) < 0$, if $k^2 = O(1)$ and $\epsilon \ll 1$. However, an instability occurs for long waves as has been shown previously for $\delta = \nu = 0$. Following the same line of reasoning, we scale the wavenumber with the square root of the amplitude of the one-dimensional wave, i.e. $k^2 = \epsilon\hat{k}^2$, upon which the eigenvalue scales with the amplitude itself: $\tau = \epsilon\hat{\tau}$. For consistency we then have to scale the horizontal velocities with $\epsilon^{1/2}$, too: $(w, \rho) = \epsilon^{1/2}(\hat{w}, \hat{\rho})$. In addition we shall see that $\tilde{\psi}_0$ and $\tilde{q}_0$ are of order ϵ. One argument comes directly from the rescaled version of (3.19*c*), which yields

$$F(M\hat{k}^2 + E\hat{\tau})\tilde{\psi}_0 = \gamma_8^0\tilde{\psi}_- + \bar{\gamma}_8^0\tilde{\psi}_+ + \mathrm{i}\lambda[\gamma_5^0(\tilde{\eta}_- - \tilde{\eta}_+) - \gamma_6^0(\tilde{u}_- - \tilde{u}_+)] + O(\epsilon), \tag{4.2}$$

where the zero superscript on the coefficients denotes their $O(1)$-approximation. But the $O(1)$-approximations to (3.26*a*) and (3.27*a*) read

$$(1 - \phi_0)\tilde{u}_+ = -\omega\tilde{\psi}_+, \qquad \phi_0\tilde{\eta}_+ = -(1 - \omega)\tilde{\psi}_+, \tag{4.3}$$

and the same relations hold for the variables with the minus index. Note that these relations correspond exactly to those for the one-dimensional solution, cf. (3.4*b*, *c*) for $\sigma = 0$. Inserting (4.3) into (4.2) and observing (A 8) and (A 10) shows immediately that

the $O(1)$-contribution to the right-hand side of (4.2) vanishes, so that either $\hat{\tau} \leqslant 0$ or $\tilde{\psi}_0 = \epsilon\hat{\psi}_0$ with $\hat{\psi}_0 = O(1)$. The latter is confirmed by looking at the rescaled versions of (3.24a), (3.25a), which give

$$B_0(\tilde{u}_0 - \tilde{\eta}_0) = b_1\tilde{\psi}_0 + O(\epsilon) = b_\delta\tilde{\psi}_0 + O(\epsilon) \Rightarrow \tilde{\psi}_0 = O(\epsilon),\ \tilde{u}_0 = \tilde{\eta}_0 + O(\epsilon). \tag{4.4}$$

Moreover, because (3.21c) becomes

$$(1-\phi_0)\hat{k}^2\,\tilde{q}_0 = (EF\hat{\tau} - G_0\hat{k}^2)\tilde{\psi}_0 + O(\epsilon), \tag{4.5}$$

we have also that $\tilde{q}_0 = \epsilon\hat{q}_0$. Implementing all these scalings into (4.1), its lowest-order approximation becomes

$$F(a_2^0\hat{\tau} + a_3|_{k^2}\hat{k}^2)\,\tilde{\psi}_+ = (\gamma_3^0 + \gamma_4^0)\tilde{u}_0\,,$$

which can be simplified to

$$\left(\hat{\tau} + \frac{a_3|_{k^2}}{a_2^0}\hat{k}^2\right)\,\tilde{\psi}_+ = -\mathrm{i}\lambda\tilde{u}_0 \tag{4.6a}$$

upon observing that $\gamma_3^0 + \gamma_4^0 = -\mathrm{i}\lambda F\,a_2^0$. Similarly,

$$\left(\hat{\tau} + \frac{\bar{a}_3|_{k^2}}{\bar{a}_2^0}\hat{k}^2\right)\,\tilde{\psi}_- = \mathrm{i}\lambda\tilde{u}_0 \tag{4.6b}$$

holds for $\tilde{\psi}_-$, so that we need only one other equation for $\tilde{u}_0$.

It can be concluded from (3.26b) and (3.27b) that $\hat{w}_0$ and $\hat{\rho}_0$ are of the same order as $\tilde{\psi}_0$, i.e. they also scale with an additional factor of ϵ. Therefore, the leading-order approximation to the perturbation variables consists of mixed modes $(\psi, q, u, w, \eta, \rho)_\pm$ and of pure transverse contributions to the vertical velocities u_0, η_0, which are moreover equal up to terms of the order of the amplitude of the one-dimensional wavetrain. Furthermore, the eigenvalue scales with the amplitude, and the critical transverse wavenumber as well as the transverse velocities scale with the square root of the amplitude.

In order to derive an equation correlating $\tilde{u}_0$ with $\tilde{\psi}_\pm$, we have to consider higher-order contributions to the equations for the pure transverse modes. At $O(\epsilon^2)$, (3.21c) gives

$$(1-\phi_0)\hat{k}^2\,\hat{q}_0 = (EF\hat{\tau} - G_0\hat{k}^2)\hat{\psi}_0 - r_q^0|_{\epsilon^2}, \tag{4.7a}$$

with

$$\begin{aligned} -r_q^0|_{\epsilon^2} = {} & FE\phi_0\mathrm{i}\hat{k}(\hat{w}_+ + \hat{w}_-) + FE(1-\phi_0)\mathrm{i}\hat{k}(\hat{\rho}_+ + \hat{\rho}_-) \\ & -B_0'\mathrm{i}\hat{k}(\hat{\rho}_+ + \hat{\rho}_- - \hat{w}_+ - \hat{w}_-) - \hat{k}^2G_0'(\tilde{\psi}_+ + \tilde{\psi}_-) + \hat{k}^2(\tilde{q}_+ + \tilde{q}_-) \\ & -\alpha_1\nu\mu\lambda\mathrm{i}\hat{k}[\lambda(\hat{\rho}_+ + \hat{\rho}_-) + \bar{\kappa}\hat{k}(\tilde{\eta}_+ - \tilde{\eta}_-)]. \end{aligned} \tag{4.7b}$$

Another relation comes from the scaled versions of (3.24a) and (3.25a):

$$\begin{gathered} \epsilon\{[F(1-\phi_0)\hat{\tau} + \mu\hat{k}^2]\tilde{u}_0 + \nu_1\hat{k}^2\tilde{\eta}_0\} + B_0(\tilde{u}_0 - \tilde{\eta}_0) = \epsilon(b_1\hat{\psi}_0 + r_{31}^{z0}|_\epsilon) + O(\epsilon^2)\,, \\ \epsilon[F\delta\phi_0\hat{\tau} + \nu_2\hat{k}^2]\tilde{\eta}_0 - B_0(\tilde{u}_0 - \tilde{\eta}_0) = \epsilon(-b_\delta\hat{\psi}_0 + r_{41}^{z0}|_\epsilon) + O(\epsilon^2)\,. \end{gathered}$$

Adding these two equations to eliminate possible $O(\epsilon)$-contributions to $\tilde{u}_0 - \tilde{\eta}_0$, and setting then $\tilde{u}_0 = \tilde{\eta}_0$ according to (4.4) leaves us with the $O(\epsilon)$-approximation

$$\begin{aligned} & [F(1-\phi_0+\delta\phi_0)\hat{\tau} + (\mu + \nu_1 + \nu_2)\hat{k}^2]\,\tilde{u}_0 \\ & \quad = (1-\delta)\hat{\psi}_0 + 2(\alpha_2 - \alpha_1)\nu\mu\frac{1+\bar{\kappa}}{\phi_0}(1-\omega)\lambda^2(\tilde{\psi}_+ + \tilde{\psi}_-), \end{aligned} \tag{4.8}$$

since most of the other terms cancel each other, partially due to (4.3). Notice that the last term vanishes, if $\alpha_1 = \alpha_2$. A third relation is obtained by combining (3.24*b*) with (3.25*b*). Writing $\hat{w}_0 = \epsilon\check{w}_0$, $\hat{\rho}_0 = \epsilon\check{\rho}_0$ according to the above results, we get the leading-order relations

$$B_0(\check{\rho}_0 - \check{w}_0) = \mathrm{i}\hat{k}[G_0\hat{\psi}_0 + (1-\phi_0)\hat{q}_0] - r_3^{y0}|_{\epsilon^{3/2}} = -\mathrm{i}\hat{k}\phi_0\hat{q}_0 + r_4^{y0}|_{\epsilon^{3/2}},$$

from which another relation between $\hat{\psi}_0$ and $\hat{q}_0$ follows, namely

$$\mathrm{i}\hat{k}(G_0\hat{\psi}_0 + \hat{q}_0) = -\mathrm{i}\hat{k}G_0'(\tilde{\psi}_+ + \tilde{\psi}_-) + (\alpha_1 - \alpha_2)v\mu\lambda[\lambda(\hat{\rho}_+ + \hat{\rho}_-) + \bar{\kappa}\hat{k}(\tilde{\eta}_+ - \tilde{\eta}_-)]\,. \tag{4.9}$$

Eliminating $\hat{q}_0$ from (4.7) and (4.9) gives us the following expression for $\hat{\psi}_0$:

$$\begin{aligned} F(E\hat{\tau} + M\hat{k}^2)\,\hat{\psi}_0 = {} & -FE\mathrm{i}\hat{k}[\phi_0(\hat{w}_+ + \hat{w}_-) + (1-\phi_0)(\hat{\rho}_+ + \hat{\rho}_-)] \\ & + B_0'\mathrm{i}\hat{k}(\hat{\rho}_+ + \hat{\rho}_- - \hat{w}_+ - \hat{w}_-) + \hat{k}^2\phi_0 G_0'(\tilde{\psi}_+ + \tilde{\psi}_-) - \hat{k}^2(\tilde{q}_+ + \tilde{q}_-) \\ & + v_3\lambda\,[\mathrm{i}\hat{k}\lambda(\hat{\rho}_+ + \hat{\rho}_-) + \mathrm{i}\bar{\kappa}\hat{k}^2(\tilde{\eta}_+ - \tilde{\eta}_-)]. \end{aligned} \tag{4.10}$$

Inserting this into (4.8) yields the desired relation between $\tilde{u}_0$ and the mixed-mode variables. Finally, using the leading-order approximations to (3.21*a*), (3.22*b*) and (3.23*b*),

$$\tilde{q}_+ = a_5^0\tilde{\psi}_+\,, \tag{4.11a}$$

$$a_{61}^0\hat{w}_+ - a_{62}^0\hat{\rho}_+ = -\mathrm{i}\hat{k}\,[(G_0 + i\lambda\mu_2)\,\tilde{\psi}_+ + (1-\phi_0)\tilde{q}_+]\,, \tag{4.11b}$$

$$a_8^0\hat{\rho}_+ - B_0\hat{w}_+ = -\mathrm{i}\hat{k}\left[\mathrm{i}\lambda(1-\omega)v_2\frac{\bar{\kappa}}{\phi_0}\tilde{\psi}_+ + \phi_0\tilde{q}_+\right], \tag{4.11c}$$

allows us to express $\tilde{q}_\pm$, $\hat{w}_\pm$, and $\hat{\rho}_\pm$ in terms of $\tilde{\psi}_\pm$. Thus (4.8) becomes

$$\begin{aligned} F(E\hat{\tau} + M\hat{k}^2)[F(1-\phi_0+\delta\phi_0)\hat{\tau} + (\mu + v_1 + v_2)\hat{k}^2]\,\tilde{u}_0 = {} & (1-\delta)\hat{k}^2(\chi\tilde{\psi}_+ + \bar{\chi}\tilde{\psi}_-) \\ & + 2(\alpha_2 - \alpha_1)v\mu\frac{1+\bar{\kappa}}{\phi_0}(1-\omega)\lambda^2 F(E\hat{\tau} + M\hat{k}^2)(\tilde{\psi}_+ + \tilde{\psi}_-)\,, \end{aligned} \tag{4.12}$$

with the complex coefficient χ being defined in Appendix D. The condition for the existence of a non-trivial solution of equations (4.6*a*, *b*) and (4.12) for $\tilde{\psi}_\pm$ and $\tilde{u}_0$ leads to the somewhat cumbersome dispersion relation

$$\begin{aligned} FE(\hat{\tau} + \xi_1\hat{k}^2)(\hat{\tau} + \tilde{\mu}\hat{k}^2)[\hat{\tau} + (\xi_2 + \mathrm{i}\xi_3)\hat{k}^2][\hat{\tau} + (\xi_2 - \mathrm{i}\xi_3)\hat{k}^2] & \\ = \frac{2(1-\delta)\lambda}{F(1-\phi_0+\delta\phi_0)}\,\hat{k}^2\,\left[\xi_5\hat{\tau} + (\xi_2\xi_5 - \xi_3\xi_4)\hat{k}^2\right] & \\ + (\alpha_1 - \alpha_2)\frac{4\lambda^3\xi_3 v\mu(1+\bar{\kappa})(1-\omega)FE}{F\phi_0(1-\phi_0+\delta\phi_0)}\hat{k}^2(\hat{\tau} + \xi_1\hat{k}^2)\,. & \end{aligned} \tag{4.13}$$

Here we have set

$$\left.\begin{aligned} \xi_1 = \frac{M}{E}, \quad \tilde{\mu} = \frac{\mu + v_1 + v_2}{F(1-\phi_0+\delta\phi_0)}, \quad \chi = \xi_4 + \mathrm{i}\xi_5, \\ \xi_2 + \mathrm{i}\xi_3 = \frac{a_3|_{k^2}}{a_2^0} = \frac{M + \mathrm{i}\lambda(\tilde{H} - \tilde{J}\omega)}{E + \tilde{J}\lambda^2 + 2\mathrm{i}\lambda(C - A\omega)}, \end{aligned}\right\} \tag{4.14}$$

so that all parameters ξ_i are real quantities. Note that the last contribution to (4.13) vanishes whenever $\alpha_1 = \alpha_2$, and that non-vanishing values of $\alpha_{1,2}$ as well as a variable viscosity of the particle phase have minor effects only, since their contributions appear only in the coefficients entering the relation (4.13) but do not alter its form which is

in complete analogy to the case $\delta = v = 0$ (Göz 1995*c*). As in that paper we may therefore conclude that the largest eigenvalue $\hat{\tau}_1$ is real and positive for small $\hat{k}$ and starts from the origin like

$$\hat{\tau}_1 = A\hat{k}^{2/3} + B\hat{k}^2 + C\hat{k}^{10/3} + O(\hat{k}^{14/3}), \tag{4.15}$$

where

$$\left.\begin{aligned} A &= (\chi_5)^{1/3}, \quad \chi_5 = \frac{1-\delta}{FE}\frac{2\lambda\xi_5}{F[1-\phi_0(1-\delta)]}, \\ B &= \frac{\chi_6 - \chi_1 A^3}{4A^3 - \chi_5}, \quad C = -A^2\frac{\chi_2 + 3\chi_1 B + 6B^2}{4A^3 - \chi_5}. \end{aligned}\right\} \tag{4.16}$$

The origin of and expressions for the χ_i are given in Appendix D. The next largest eigenvalue is also real for small $\hat{k}$ and is given by

$$\hat{\tau}_2 = -(\chi_6/\chi_5)\hat{k}^2 + O(\hat{k}^6) \quad (\hat{k} \ll 1), \quad \chi_6/\chi_5 = (\xi_2\xi_5 - \xi_3\xi_4)/\xi_5. \tag{4.17}$$

If $\chi_6 < 0$, $\hat{\tau}_2$ is positive for small $\hat{k}$ and will merge with $\hat{\tau}_1$ at a point above the axis $\mathrm{Re}(\hat{\tau}) = 0$ to form a complex-conjugate pair. If $\chi_6 > 0$, $\hat{\tau}_2$ falls off from 0 at $\hat{k} = 0$ but may rise again to merge with $\hat{\tau}_1$ above or below the axis $\mathrm{Re}(\hat{\tau}) = 0$; in the former case $\hat{\tau}_2$ crosses the axis at a wavenumber given by

$$\hat{k}_c^4 = \chi_6/\chi_4 \;\sim\; \xi_2\xi_5 - \xi_3\xi_4 \tag{4.18}$$

(this requires $\chi_6 > 0$ because χ_4 is always positive). If the second branch stays below the axis, the leading eigenvalue will be real and positive in the interval $\hat{k} \in (0, \hat{k}_c)$, so that stabilization occurs at the critical wavenumber $\hat{k}_c$.

The small-$\hat{k}$ behaviour of the two remaining eigenvalues is given by

$$\hat{\tau}_{3,4} = (-1 \pm \mathrm{i}\sqrt{3})(\chi_5)^{1/3}\hat{k}^{2/3}/2 + O(\hat{k}^2) \quad (\hat{k} \ll 1); \tag{4.19}$$

they have negative real parts for all $\hat{k}$. Ultimately all eigenvalues must stabilize, because the short-wave analysis of (4.13) shows that their asymptotic behaviour is given by

$$\hat{\tau}_{(1,2,3,4)} \sim (-\xi_1, -\tilde{\mu}, -\xi_2 \mp \mathrm{i}\xi_3)\hat{k}^2 \quad (\hat{k} \gg 1). \tag{4.20}$$

At intermediate values of $\hat{k}$, these four eigenvalues interact in a variety of ways, and we will not attempt to enumerate them. Instead, we present two specific examples corresponding to an air-fluidized bed (figure 4) and a water-fluidized bed (figure 5), both with $\phi_c = 0.424$ (see tables 1 and 2). In figure 4, the dominant eigenvalue is real. The next largest eigenvalue is also real for small $\hat{k}$, while the other two form a complex-conjugate pair (only the real part of this pair is shown). In this example, there is no interaction between the largest and the three other eigenvalues; such interactions do occur for other values of ϕ_c and/or when a variable bulk modulus, $G_0' \neq 0$, is taken into account.

In the water-fluidized bed example, figure 5, the two leading real eigenvalues ($\hat{\tau}_1$ and $\hat{\tau}_2$) interact to produce a complex-conjugate pair. On the other hand, the initially complex-conjugate pair ($\hat{\tau}_3$ and $\hat{\tau}_4$) split into a pair of real eigenvalues, one of which rapidly falls off to $-\infty$, while the other increases towards the two leading eigenvalues before decreasing again, after some interaction.

It is revealing to compare figures 4 and 5. These figures provide us with the growth rates of two-dimensional perturbations of plane vertically travelling fully developed waves near their onset and we have to keep in mind that this growth rate and

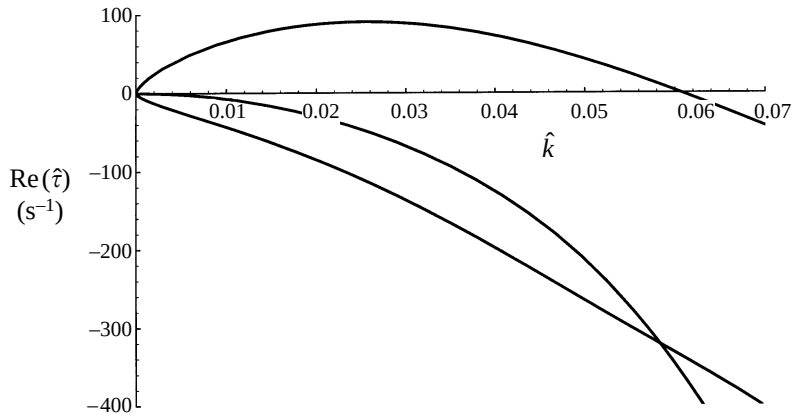

FIGURE 4. Dimensional secondary growth rates, scaled with the amplitude, vs. the scaled transverse wavenumber for an air-fluidized bed with $\phi_c = 0.424$ (see tables 1 and 2). The real parts of the four eigenvalues $\hat{\tau}_{1,2,3,4}$ obtained by solving (4.13) are plotted against $\hat{k}$.

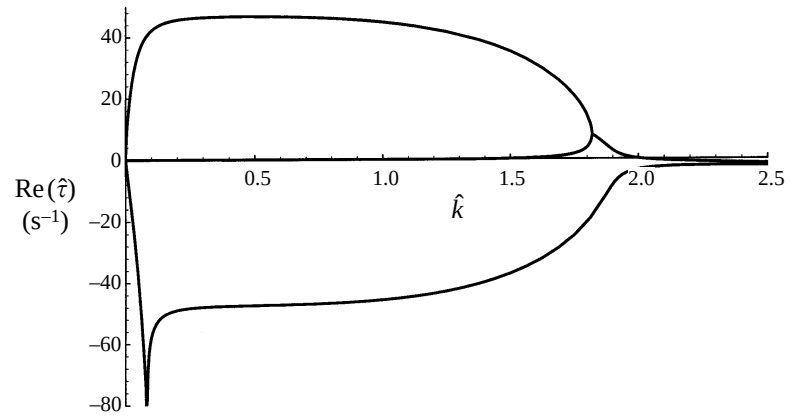

FIGURE 5. Dimensional secondary growth rates $\mathrm{Re}(\hat{\tau}_{1,2,3,4})$, scaled with the amplitude, vs. the scaled transverse wavenumber $\hat{k}$ for a water-fluidized bed with $\phi_c = 0.424$ (see tables 1 and 2).

square of the transverse wavenumber have been scaled with the amplitude of the one-dimensional wave. One can readily see from these figures that for a given amplitude of the one-dimensional wave the difference in the dimensional growth rates of air- and water-fluidized beds is much smaller than that in the primary growth rates.

5. Discussion

We have examined in this paper the primary and secondary instabilities in air- and water-fluidized beds for various parameter values. The overall tendency is that the primary growth rates are vastly different while the amplitude-related secondary growth rates are roughly comparable. We have shown that the growth rate of the primary instability scales as $\rho_s u_0^2/\mu_s^0$, which explains the differences observed between these two beds.

The Froude number appearing in the model equations is in terms of quantities which can be directly measured; in contrast, the Reynolds number involves particle-phase viscosity, μ_s^0, and there is some uncertainty in our ability to estimate its value.

In their analysis of the dynamics of air- and water-fluidized beds of glass beads, Anderson *et al.* (1995) assumed the particle-phase viscosities of the two beds to be equal. In that case, then, our finding shows that the growth rates of the two beds will differ by a factor determined by the square of the fluidization velocity. This is indeed confirmed by numerical calculations. Writing $R = (\rho_s r_p/\mu_s^0)(g r_p F)^{1/2}$, we see that for both the air- and water-fluidized beds listed in table 1, $R = 0.019\,F^{1/2}$.

5.1. *Scaling behaviour of the secondary growth rates*

In order to bring forth the dependence of the growth rate of the secondary instability on R and, particularly, F, let us consider the specific example of $\phi_0 = 0.43$, $\phi_c = 0.424$, $n = 3$, $\delta = v = 0$. Then the kinematic wave velocity d appearing in (3.7) is 2.85, and the dynamic wave velocity of the travelling wave emerging from the uniform solution at the Hopf bifurcation point is $\omega_0 = 2.7226$; both are measured in terms of the fluidization velocity u_0 (which is determined implicitly by (2.4)). Now consider fully developed small-amplitude (ϵ), one-dimensional vertically travelling wave solutions and their stability to transverse perturbations. The largest dimensionless eigenvalue, $\tau_1 = \epsilon\hat{\tau}_1$, for small dimensionless lateral wavenumber, $k = \epsilon^{1/2}\hat{k}$, is given by the solution with largest real part of the dispersion relation (4.13). While it is virtually impossible to determine the maximum of the growth rate, $\hat{\tau}_{max}$, analytically, we may obtain an estimate of it by considering the small-$\hat{k}$ expansion (4.15):

$$\hat{\tau}_1 = A\hat{k}^{2/3} + B\hat{k}^2 + C\hat{k}^{10/3} + O(\hat{k}^{14/3})\,.$$

Considering only the first two terms of this expansion, we can readily estimate the value $\hat{k}_m^0$ at which the maximum growth rate occurs and also find its magnitude, $\hat{\tau}_m^0$, namely

$$\hat{k}_m^0 = \left(-\frac{A}{3B}\right)^{3/4}, \quad \hat{\tau}_m^0 = \tfrac{2}{3}A\left(-\frac{A}{3B}\right)^{1/2}. \tag{5.1}$$

Obviously this is valid only if B is negative (A is positive here), which is found to be true in our cases. We could repeat the exercise including the third term in the above expansion to find the conditions

$$(\hat{k}_m^{\pm})^{4/3} = (-3B \pm (9B^2 - 20AC)^{1/2})/(10C) > 0, \quad 9B^2 - 20AC > 0, \tag{5.2}$$

from which $\hat{\tau}_m^{\pm}$ would follow. The inequality conditions in (5.2), however, are not always satisfied and therefore the seemingly better approximation less useful. In the air-fluidized bed example (table 1) for which $C < 0$, (5.1) was found to be a very good approximation for both $\hat{k}_m^0$ and $\hat{\tau}_m^0$; in contrast, in the water-fluidized bed example for which $C > 0$, (5.1) proved to be a good estimate of the maximum growth rate $\hat{\tau}_m^0$, but not $\hat{k}_m^0$ (this has to do with the range of validity of the small-$\hat{k}$ expansion of $\hat{\tau}_1$, cf. figures 4 and 5). This observation led us to view (5.1*b*) as an acceptable approximation for the maximum secondary growth rate and examine the dependence of A and B on the model parameters R and F. The full expressions for the expansion coefficients and growth rates are unwieldy but one can easily derive asymptotic expressions. For small Froude number we get

$$\left.\begin{aligned} A &= 4.634/F^{1/3} - 34.09\,RF^{2/3} + 1072.7\,R^2F^{5/3} - \ldots, \\ B &= -0.585/R - 2.745\,F + 12.12\,RF^2 - \ldots, \\ \hat{k}_m^0 &= 2.072\,R^{3/4}/F^{1/4} - 18.73\,R^{7/4}F^{3/4} + \ldots, \\ \hat{\tau}_m^0 &= 5.021\,(R/F)^{1/2} - 67.19\,R^{3/2}F^{1/2} + 2069\,R^{5/2}F^{3/2} - \ldots; \end{aligned}\right\} \tag{5.3}$$

and in the limit of large Froude number

$$\left.\begin{aligned} A &= 3.502/F^{1/3} + 0.039/(RF^{4/3}) - 0.0015/(R^2F^{7/3}) + \ldots, \\ B &= -1.063\,F - 3.762/R + 10.1/(FR^2) - \ldots, \\ \hat{k}_m^0 &= 1.073/F - 2.841/(RF^2) + 16.46/(R^2F^3) + \ldots, \\ \hat{\tau}_m^0 &= 2.447/F - 4.291/(RF^2) + 23/(R^2F^3) - \ldots. \end{aligned}\right\} \tag{5.4}$$

Note that the leading-order terms in (5.4) are independent of the Reynolds number. The above are dimensionless expressions; to get the dimensional growth rates, $\hat{\tau}_1$ etc. has to be multiplied by $u_0/r_p = (Fg/r_p)^{1/2}$. If we now assume the particle-phase viscosity to be a constant so that $R \sim F^{1/2}$, and examine the asymptotic behaviour for small and large Froude number, the leading-order dimensional terms are found to scale as follows:

$$A_d \sim F^{1/6},\ B_d \sim -O(1),\ \hat{k}_m^0 \sim F^{1/8},\ \hat{\tau}_{m,d}^0 \sim F^{1/4} \quad (F \ll 1); \tag{5.5}$$

$$A_d \sim F^{1/6},\ B_d \sim -F^{3/2},\ \hat{k}_m^0 \sim F^{-1},\ \hat{\tau}_{m,d}^0 \sim F^{-1/2} \quad (F \gg 1). \tag{5.6}$$

We see that the dependence on F is especially weak for small Froude number, and that the same is true for the initial rise of the growth rate with the wavenumber (described by the coefficient A_d) in the limit of large F. Note that the growth rate of the secondary instability increases with Froude number (only weakly) when $F \ll 1$, but it reverses the trend when $F \gg 1$. (The same trend holds for the lateral wavenumber corresponding to the maximum growth rate.) This should be contrasted with the primary growth rate which increases with F as long as the approximation (3.10) is valid.

A surprisingly good approximation of $\hat{\tau}_{m,d}^0$ is obtained by patching together the leading-order terms for small and large Froude numbers in the following way:

$$\hat{\tau}_{as}^{-1} = \hat{\tau}_{s1}^{-1} + \hat{\tau}_{l1}^{-1}, \tag{5.7}$$

where $\hat{\tau}_{s1} = 5.021(g/r_p)^{1/2}R^{1/2}$, $\hat{\tau}_{l1} = 2.447(g/r_p)^{1/2}F^{-1/2}$. See figure 6. This figure also shows that the (approximate) dimensional secondary growth rates differ at most by a factor of 10 for Froude numbers between 10^{-4} and 10^2, say. For the air- and water-fluidized bed examples in table 1, the values of $\hat{\tau}_{m,d}^0$ are 91.1 s^{-1} and 40.5 s^{-1}, respectively, very close to the exact values, cf. figures 4 and 5. Now that we found the leading-order terms of A, B and $\hat{\tau}_m^0$ to give reliable approximations it is worthwhile to calculate their general forms for $\delta = v = 0$:

$$\left.\begin{aligned} A &= \left[\frac{2d(d-\omega_0+\phi_0)^2}{(d-\omega_0)\phi_0(1-\phi_0)^2}\right]^{1/3} F^{-1/3} + \ldots, \\ B &= -\frac{1}{3(1-\phi_0)R} - \ldots \quad \text{for } F \ll 1, \end{aligned}\right\} \tag{5.8}$$

and

$$\left.\begin{aligned} A &= \left[2\frac{\omega_0\phi_0 + (d+\phi_0)(d-\omega_0+\phi_0)}{\phi_0(1-\phi_0)^2}\right]^{1/3} F^{-1/3} + \ldots \\ B &= -(\omega_0^2\phi_0/3)F + \ldots \quad \text{for } F \gg 1, \end{aligned}\right\} \tag{5.9}$$

from which $\hat{\tau}_m^0$ can be obtained via (5.1).

5.2. *Comparison of primary and secondary growth rates*

Let us recall from §3.1 that the dimensionless maximum primary growth rate for weakly unstable beds scales with the Reynolds number, $\sigma_m \sim R$. Using the asymptotic

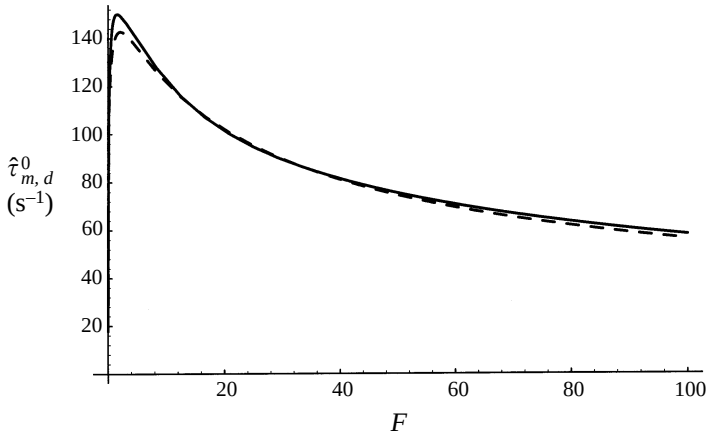

FIGURE 6. Dimensional maximum growth rate $\hat{\tau}^0_{m,d}$ based on (5.1) vs. the Froude number (solid curve), and its inverse-mean approximation (5.7) by the first-order asymptotic terms for small and large Froude number (broken curve).

expressions for the growth rate of the secondary instability ($\tau_m = \epsilon\hat{\tau}_m$ with $\hat{\tau}_m \approx \hat{\tau}^0_m$ given by (5.3) and (5.4)),

$$\frac{\tau_m}{\sigma_m} \sim \begin{cases} \epsilon(RF)^{-1/2} & \text{for } F \ll 1 \\ \epsilon(RF)^{-1} & \text{for } F \gg 1. \end{cases} \tag{5.10}$$

One can extract from these expressions a scale for the amplitude of the one-dimensional wave for which $\tau_m \sim \sigma_m$:

$$\epsilon_{cm} \sim \begin{cases} 0.001747\,(RF)^{1/2}, & F \ll 1 \\ 0.003585\,RF, & F \gg 1. \end{cases} \tag{5.11}$$

One can therefore expect that the secondary instability will set in at very small amplitudes in liquid-fluidized beds, while in gas-fluidized beds the one-dimensional wave has to grow to a much larger amplitude before the secondary instability will take over. This was indeed seen in the numerical simulations of Anderson *et al.* (1995), and our analytical work establishes the Froude number as the correct scale.

It is clear from experimental studies of instabilities in fluidized beds (Anderson & Jackson 1968; El-Kaissy & Homsy 1976; Didwania & Homsy 1981; Nicolas *et al.* 1996) that non-uniform structures are initiated near the bottom distributor and that these structures grow while being convected up through the bed. An initial non-uniformity having a plane wave structure will become unstable to transverse perturbations when its voidage amplitude reaches a critical value, ϵ_c, given by

$$\epsilon_c = (2\pi/b\hat{k}_c)^2, \tag{5.12}$$

where the bed width b is measured in multiples of the particle radius and $\hat{k}_c$ is the largest wavenumber for which a secondary instability can occur ($\mathrm{Re}\,(\hat{\tau}_1) = 0$). This wavenumber is given by (4.18) if $\hat{\tau}_1$ is a real eigenvalue in the whole interval $[0, \hat{k}_c]$; otherwise (4.18) gives the point at which the second eigenvalue $\hat{\tau}_2$ crosses the real axis from below, so that stabilization occurs at a wavenumber larger than $\hat{k}_c$. For the parameters used here we find that the transition point occurs at $F^* \approx 0.67$, i.e. $\hat{\tau}_1$ is real and positive for $\hat{k} \in (0, \hat{k}_c(F))$ for $F > F^*$, but forms a complex-conjugate pair with $\hat{\tau}_2$ before stabilizing for $F < F^*$; in the latter case we use $\hat{k}_c$ simply as lower

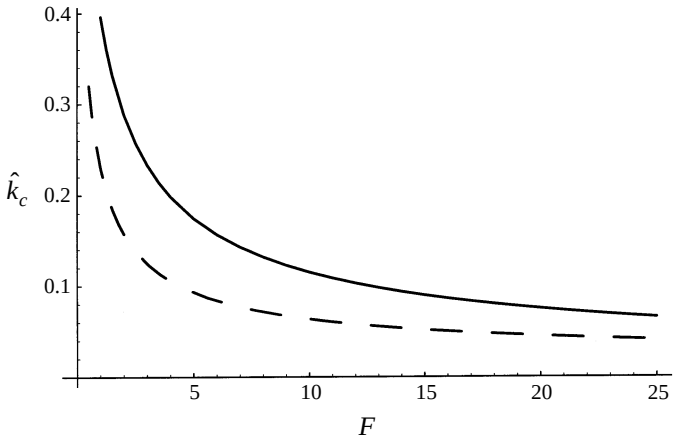

FIGURE 7. Froude number dependence of $\hat{k}_c$ according to (4.18). The solid curve represents the case $\delta = \nu = 0$ which is almost identical to the curve for the air-fluidized bed, the broken curve represents the water-fluidized bed case.

bound for the actual stabilization point. A plot of $\hat{k}_c$ over the full range of Froude numbers is presented in figure 7, where we have set $R = 0.019\,F^{1/2}$. Asymptotically, this quantity behaves like

$$\hat{k}_c \sim \begin{cases} 3.297\,(R/F)^{1/2} \sim F^{-1/4}, & F \ll 1 \\ 1.321\,(R/F^3)^{1/4} \sim F^{-5/8}, & F \gg 1 \end{cases} \tag{5.13}$$

from which the asymptotic scaling behaviour of the corresponding amplitude follows:

$$\epsilon_c \sim \begin{cases} 3.63 \times 10^{-6} \times F/R \sim F^{1/2}, & F \ll 1 \\ 2.26 \times 10^{-5} \times (F^3/R)^{1/2} \sim F^{5/4}, & F \gg 1. \end{cases} \tag{5.14}$$

The expression (5.12) for ϵ_c with $b = 10^3$ and $\hat{k}_c$ from (4.18) is plotted together with $\epsilon_{cm} = \sigma_m/\hat{\tau}_m^0$ in figure 8. The two curves for ϵ_{cm} and ϵ_c have similar shape and lie close together for a wide range of Froude numbers. They will move further apart, however, for narrower beds; in addition, the asymptotic analysis shows that ϵ_{cm} will become smaller than ϵ_c at a small enough Froude number (≈ 0.39 for a bed width of 500 particle diameters). Most important is the monotonic rise of both ϵ_c and ϵ_{cm} with the Froude number, showing that the critical amplitude in the liquid-fluidized bed is much smaller than in the gas-fluidized bed, thereby confirming the results of our consideration of initial secondary growth rates in §3.3.

Let us now consider gas- and liquid-fluidized beds with the same particle size and bed width and ask how long it is going to take the fastest growing one-dimensional wave to rise from a certain initial amplitude ϵ_0 to a critical amplitude such that the given bed width corresponds to either the maximum growth rate or marginal stability of transverse perturbations. In the linear approximation, this time is given by

$$\Delta t = \ln(\epsilon/\epsilon_0)/\sigma_m \quad (\epsilon = \epsilon_c \text{ or } \epsilon_{cm}). \tag{5.15}$$

Asymptotically, $\epsilon \sim aF^b$, with appropriate values of a and b according to (5.11) and (5.14), so that with $R \sim F^{1/2}$ the dimensional time scale becomes

$$\Delta t_d \sim (\ln a - \ln \epsilon_0 + b \ln F)/F. \tag{5.16}$$

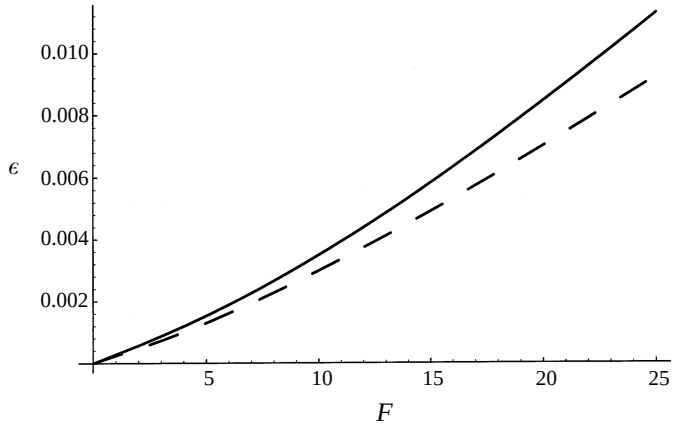

FIGURE 8. Froude number dependence of the amplitudes ϵ_c (broken curve) and ϵ_{cm} (solid curve) for a bed width of 500 particle diameters.

The corresponding dimensional travelling distance is then given by

$$\Delta s_d = \Delta t_d \, u_0 \, \omega \approx \Delta t \, r_p \omega_0 \sim (\ln a - \ln \epsilon_0 + b \ln F)/F^{1/2} \tag{5.17}$$

and behaves similarly to $\Delta t(F)$. Of course, these estimates make sense only if $\epsilon > \epsilon_0$; in other words, if the initial disturbance is large enough, the secondary instability would set in right away. This sets a critical Froude number of $F_c = (\epsilon_0/a)^{1/b}$, above (below) which the above estimates are valid for $b > 0$ ($b < 0$). Assuming a very small ϵ_0, and ϵ_c or ϵ_{cm} as critical amplitudes, Δt_d becomes positive at a very small F_c, rises sharply to a considerable maximum (still at a small F) and afterwards declines toward 0 as $F \to \infty$. For an ϵ_0 of the order of 10^{-6}, both the air- and water-fluidized beds considered repeatedly in this paper lie on the declining part of the curve (5.16). With increasing value of ϵ_0, the critical Froude number F_c increases also until it exceeds even the Froude number value of the air-fluidized bed. Using for instance the expression for ϵ_c in (5.15), we can calculate critical values of ϵ_0 and obtain 9.95×10^{-6} and 1.07×10^{-2} for the water- and air-fluidized beds of table 1, respectively. These values lie in the same range as those found in §3.3 for the critical amplitudes v_p^c for which the initial secondary growth rates become comparable to the primary ones thus further confirming the validity of our asymptotic analysis.

6. Conclusions

The major accomplishments of this study are as follows.

We have identified $\rho_s u_0^2/\mu_s^0$ (times a factor that measures the strength of the instability) as the appropriate scale for the growth rate of the primary instability in weakly unstable uniformly fluidized beds. This gives a possible explanation of why these growth rates are so vastly different for typical air- and water-fluidized beds.

The initial dimensional growth rates of transverse perturbations imposed on growing one-dimensional plane travelling wave solutions of small amplitude in water- and air-fluidized beds are found to be of comparable magnitude, but the critical amplitude of the one-dimensional wave at which the secondary growth rate begins to exceed the primary growth rate is much larger in the air-fluidized bed.

A closer look at the growth rate of the secondary instability of fully developed small-amplitude one-dimensional travelling waves exposed the Froude number dependence

of this mode, explaining why these growth rates are similar for the water- and air-fluidized beds.

Finally, we considered two different ways of analysing the critical amplitude of one-dimensional travelling waves at which the secondary instability will begin to take over and found both to yield similar estimates. In the water-fluidized bed example considered the secondary instability sets in at a much smaller amplitude than in the air-fluidized bed. However, the dimensional time and distance travelled by the one-dimensional wave having a very small initial amplitude before the secondary structure is observed are larger for the water-fluidized bed, and this is consistent with experimental observations.

M.F.G. gratefully acknowledges the support by a fellowship from the Deutsche Forschungsgemeinschaft under grant nos. Go 605/3-1, -2.

Appendix A

The nonlinear terms of §2 are given by

$$\boldsymbol{R}_3 = \boldsymbol{R}_{31} + \boldsymbol{R}_{32} + \boldsymbol{R}_{33}, \quad \boldsymbol{R}_4 = \boldsymbol{R}_{41} + \boldsymbol{R}_{42} + \boldsymbol{R}_{43}, \tag{A 1}$$

where the quadratic terms appearing in (2.6c, d) are collected in the expressions

$$\begin{aligned}\boldsymbol{R}_{31} = {} & F\tilde{\phi}(\partial_t\tilde{\boldsymbol{v}} - \omega\boldsymbol{k}\cdot\nabla\tilde{\boldsymbol{v}}) - F(1-\phi_0)\tilde{\boldsymbol{v}}\cdot\nabla\tilde{\boldsymbol{v}} + B_0'\tilde{\phi}(\tilde{\boldsymbol{u}} - \tilde{\boldsymbol{v}}) + \tfrac{1}{2}B_0''\tilde{\phi}^2\boldsymbol{k} \\ & + \tilde{\phi}\nabla\tilde{p} - G_0'\tilde{\phi}\nabla\tilde{\phi} - \alpha_1 v\mu\tilde{\phi}(\Delta + \bar{\kappa}\nabla\nabla\cdot)\tilde{\boldsymbol{u}} \\ & + \frac{\mu}{\mu_s^0}\nabla\cdot\{\lambda_s'^0\tilde{\phi}\,(\nabla\cdot\tilde{\boldsymbol{v}})\boldsymbol{I} + \mu_s'^0\tilde{\phi}\,[\nabla\tilde{\boldsymbol{v}} + (\nabla\tilde{\boldsymbol{v}})^T - \tfrac{2}{3}(\nabla\cdot\tilde{\boldsymbol{v}})\boldsymbol{I}]\}, \end{aligned} \tag{A 2a}$$

$$\begin{aligned}\boldsymbol{R}_{41} = {} & -F\delta\tilde{\phi}\,[\partial_t\tilde{\boldsymbol{u}} + (1-\omega)\boldsymbol{k}\cdot\nabla\tilde{\boldsymbol{u}}] - F\delta\phi_0\tilde{\boldsymbol{u}}\cdot\nabla\tilde{\boldsymbol{u}} - B_0'\tilde{\phi}(\tilde{\boldsymbol{u}} - \tilde{\boldsymbol{v}}) \\ & - \tilde{\phi}\nabla\tilde{p} - \tfrac{1}{2}B_0''\tilde{\phi}^2\boldsymbol{k} + \alpha_2 v\mu\tilde{\phi}(\Delta + \bar{\kappa}\nabla\nabla\cdot)\tilde{\boldsymbol{u}}, \end{aligned} \tag{A 2b}$$

while the cubic terms are given by

$$\begin{aligned}\boldsymbol{R}_{32} = {} & F\tilde{\phi}\tilde{\boldsymbol{v}}\cdot\nabla\tilde{\boldsymbol{v}} + \tfrac{1}{2}B_0''\tilde{\phi}^2(\tilde{\boldsymbol{u}} - \tilde{\boldsymbol{v}}) + \tfrac{1}{6}B_0'''\tilde{\phi}^3\boldsymbol{k} - \tfrac{1}{2}G_0''\tilde{\phi}^2\nabla\tilde{\phi} \\ & + \frac{\mu}{2\mu_s^0}\nabla\cdot\{\lambda_s''^0\tilde{\phi}^2\,(\nabla\cdot\tilde{\boldsymbol{v}})\boldsymbol{I} + \mu_s''^0\tilde{\phi}^2\,[\nabla\tilde{\boldsymbol{v}} + (\nabla\tilde{\boldsymbol{v}})^T - \tfrac{2}{3}(\nabla\cdot\tilde{\boldsymbol{v}})\boldsymbol{I}]\}, \end{aligned} \tag{A 3a}$$

$$\boldsymbol{R}_{42} = -F\delta\tilde{\phi}\tilde{\boldsymbol{u}}\cdot\nabla\tilde{\boldsymbol{u}} - \tfrac{1}{2}B_0''\tilde{\phi}^2(\tilde{\boldsymbol{u}} - \tilde{\boldsymbol{v}}) - \tfrac{1}{6}B_0'''\tilde{\phi}^3\boldsymbol{k}. \tag{A 3b}$$

The higher-order terms are of the form

$$\boldsymbol{R}_{43} = O(\tilde{\phi}^4)\,\boldsymbol{k} + O(\tilde{\phi}^3)(\tilde{\boldsymbol{u}} - \tilde{\boldsymbol{v}}),\ \boldsymbol{R}_{33} = O(\tilde{\phi}^3)\nabla\tilde{\phi} + \nabla\cdot[O(\tilde{\phi}^3)\nabla\tilde{\boldsymbol{v}}] - \boldsymbol{R}_{43}. \tag{A 4}$$

Furthermore,

$$R_p = FE[(1-\phi_0)R_2 - \phi_0 R_1] - F\dot{R}_1 + F\omega R_1' + c\Delta R_1 + \alpha_1 FH\Delta R_2 + \nabla\cdot\boldsymbol{R}_3, \tag{A 5}$$

$$\begin{aligned}R_\phi = {} & E[(1-\phi_0)R_2 - \phi_0 R_1] + \delta(1-\phi_0)\dot{R}_2 - \phi_0\dot{R}_1 \\ & + \delta(1-\phi_0)(1-\omega)R_2' + \phi_0\omega R_1' + (\tilde{J} - \tilde{H})\Delta R_1 - \tilde{H}\Delta R_2 \\ & + F^{-1}[\phi_0\,\nabla\cdot\boldsymbol{R}_3 - (1-\phi_0)\,\nabla\cdot\boldsymbol{R}_4], \end{aligned} \tag{A 6}$$

$$\boldsymbol{R}_v = \boldsymbol{R}_3 + \frac{\mu\kappa}{1-\phi_0}\nabla R_1 + \nu_1\frac{\bar{\kappa}}{\phi_0}\nabla R_2, \quad \boldsymbol{R}_u = \boldsymbol{R}_4 + \frac{\nu_2\bar{\kappa}}{\phi_0}\nabla R_2. \tag{A 7}$$

The constants appearing in §2 and above are defined as follows:

$$b_1 = 1 + B_0' + p_0', \quad b_\delta = \delta + B_0' + p_0'; \tag{A 8a}$$

$$v_1 = \alpha_1 v\mu(1-\phi_0), \quad v_2 = v\mu[1-\alpha_2(1-\phi_0)]; \tag{A 8b}$$

$$c_1 = \hat{c} - \alpha_1 FH, \quad \hat{c} = \frac{\mu(1+\kappa)}{1-\phi_0}, \quad H = \frac{v(1+\bar{\kappa})(1-\phi_0)}{R\phi_0}; \tag{A 9}$$

$$\left.\begin{aligned} &A = \phi_0 + C,\ C = \delta(1-\phi_0),\ E = \frac{B_0}{F\phi_0(1-\phi_0)} \doteq \frac{1-\delta}{F},\ M = \frac{\phi_0|G_0|}{F}, \\ &D = \frac{1}{F}\left[\frac{B_0}{\phi_0} - B_0' + (1-\delta)(1-2\phi_0)\right] \doteq (n+2)(1-\phi_0)(1-\delta)/F, \\ &\tilde{H} = H[1-\alpha_1\phi_0 - \alpha_2(1-\phi_0)], \quad \tilde{J} = J - H + \tilde{H}, \quad J = \frac{\phi_0\hat{c}}{F} + H, \end{aligned}\right\} \tag{A 10}$$

in notational consistency with Göz (1992); the symbol $\doteq$ denotes the expression obtained upon using the drag coefficient (2.2). Notice that $\tilde{H} = H$ for $\alpha_{1,2} = 0$, whilst $\tilde{H} = 0$ for $\alpha_{1,2} = 1$. Finally, the constants of (2.10) are

$$\mu_1 = \frac{\mu\kappa}{1-\phi_0} - v_1\frac{\bar{\kappa}}{\phi_0}, \quad \mu_2 = \frac{\mu\kappa\omega}{1-\phi_0} + v_1(1-\omega)\frac{\bar{\kappa}}{\phi_0} = \mu_1\omega + v_1\frac{\bar{\kappa}}{\phi_0}. \tag{A 11}$$

Appendix B

This Appendix lists the functional expressions and constants omitted in §3.2. The various constants a_i appearing in §3 are given by

$$\left.\begin{aligned} &a_1 = 1 + B_0' + p_0' - B_0/\phi_0 + (EF + c_1k^2)\omega + \alpha_1 FHk^2, \\ &a_2 = E + \tilde{J}(\lambda^2+k^2) + 2\mathrm{i}\lambda(C - A\omega), \\ &a_3 = M(\lambda^2+k^2) - (A\omega^2 - 2C\omega + C)\lambda^2 + \mathrm{i}\lambda[D - E\omega + (\tilde{H} - \tilde{J}\omega)(\lambda^2+k^2)], \\ &a_4 = [EF + c_1(\lambda^2+k^2) - 2\mathrm{i}\lambda F\omega]/[(1-\phi_0)(\lambda^2+k^2)], \\ &a_5 = -\{F\omega^2\lambda^2 + G_0(\lambda^2+k^2) + \mathrm{i}\lambda[a_1 + (c_1\omega + \alpha_1 FH)\lambda^2]\}/[(1-\phi_0)(\lambda^2+k^2)], \\ &a_{61} = B_0 + \mu(\lambda^2+k^2) - \mathrm{i}\lambda F\omega(1-\phi_0), \quad a_{62} = B_0 - v_1(\lambda^2+k^2), \\ &a_7 = b_1 + \mu_2\lambda^2 - \mathrm{i}\lambda G_0, \quad a_8 = B_0 + v_2(\lambda^2+k^2) + \mathrm{i}\lambda F\delta\phi_0(1-\omega), \\ &a_9 = b_\delta - v_2\frac{\bar{\kappa}}{\phi_0}\lambda^2(1-\omega). \end{aligned}\right\} \tag{B 1}$$

The $r_{\psi,q}$ denote the linearizations of the nonlinear terms $R_{\phi,p}$ at the one-dimensional solution, applied to the perturbation vector (3.11), and the $r_{(u,w),(\eta,\rho)}$ denote those of $\boldsymbol{R}_{\boldsymbol{v},\boldsymbol{u}}$:

$$\begin{aligned} r_\psi = {} & \mathrm{i}k[\phi_0 r_3^y - (1-\phi_0)r_4^y] + [\phi_0 r_3^z - (1-\phi_0)r_4^z]' \\ & -F[\phi_0\dot{r}_1 - \delta(1-\phi_0)\dot{r}_2] + F[\omega\phi_0 r_1 + \delta(1-\phi_0)(1-\omega)r_2]' \\ & -(FE + ck^2)\phi_0 r_1 + F[E(1-\phi_0) + \tilde{H}k^2]r_2 + (c\phi_0 r_1 - F\tilde{H}r_2)'', \end{aligned} \tag{B 2}$$

$$\begin{aligned} r_q = {} & -FE[\phi_0 r_1 - (1-\phi_0)r_2] - F\dot{r}_1 + F\omega r_1' + cr_1'' - ck^2 r_1 + r_3^{z\prime} + \mathrm{i}kr_3^y \\ & +\alpha_1 FH(r_2'' - k^2 r_2), \end{aligned} \tag{B 3}$$

$$r_u = r_3^z + \frac{\mu\kappa}{1-\phi_0}r_1' + v_1\frac{\bar{\kappa}}{\phi_0}r_2', \quad r_w = \mathrm{i}k\left[\frac{\mu\kappa}{1-\phi_0}r_1 + v_1\frac{\bar{\kappa}}{\phi_0}r_2\right] + r_3^y, \tag{B 4}$$

$$r_\eta = r_4^z + v_2\frac{\bar{\kappa}}{\phi_0}r_2', \quad r_\rho = r_4^y + v_2\frac{\bar{\kappa}}{\phi_0}\mathrm{i}kr_2. \tag{B 5}$$

The functionals bearing a superscript zero are those obtained by averaging over a period in z, i.e.

$$r_u^0 = r_{31}^{z0}, \quad r_\eta^0 = r_{41}^{z0}, \tag{B 6}$$

$$r_w^0 = \mathrm{i}k\left[\frac{\mu\kappa}{1-\phi_0}r_1^0 + v_1\frac{\bar{\kappa}}{\phi_0}r_2^0\right] + r_{31}^{y0}, \quad r_\rho^0 = r_{41}^{y0} + v_2\frac{\bar{\kappa}}{\phi_0}\mathrm{i}kr_2^0. \tag{B 7}$$

Here, the r_i denote the linearizations of the R_i and are given by

$$r_1 = \mathrm{i}k\phi_1 w + (\phi_1 u + v_1\psi)', \quad r_2 = -\mathrm{i}k\phi_1\rho - (\phi_1\eta + u_1\psi)', \tag{B 8}$$

and $\boldsymbol{r}_3 = \boldsymbol{r}_{31} + \boldsymbol{r}_{32} + O(\phi_1^3)$, $\boldsymbol{r}_4 = \boldsymbol{r}_{41} + \boldsymbol{r}_{42} + O(\phi_1^3)$, with

$$\begin{aligned} r_{31}^y = {} & F\phi_1\dot{w} - F[(1-\phi_0)v_1 + \omega\phi_1]w' + B_0'\phi_1(\rho - w) - \mathrm{i}kG_0'\phi_1\psi + \mathrm{i}k\phi_1 q \\ & -\alpha_1 v\mu\phi_1[\rho'' - k^2\rho + \mathrm{i}k\bar{\kappa}(\eta' + \mathrm{i}k\rho)] \\ & +\frac{\mu}{\mu_s^0}\{\mathrm{i}k(\lambda_s'^0 - \tfrac{2}{3}\mu_s'^0)[v_1'\psi + \phi_1(u' + \mathrm{i}kw)] + \mu_s'^0\{[\phi_1(w' + \mathrm{i}ku)]' - 2k^2\phi_1 w\}\}, \end{aligned} \tag{B 9a}$$

$$\begin{aligned} r_{31}^z = {} & F\phi_1\dot{u} - F(1-\phi_0)v_1'u - F[(1-\phi_0)v_1 + \omega\phi_1]u' + F(\dot{v}_1 - \omega v_1')\psi \\ & +B_0'\phi_1(\eta - u) + [B_0'(u_1 - v_1) + B_0''\phi_1]\psi - G_0'(\phi_1\psi)' + p_1'\psi + \phi_1 q' \\ & -\alpha_1 v\mu\{\phi_1[\eta'' - k^2\eta + \bar{\kappa}(\mathrm{i}k\rho + \eta')'] + (1+\bar{\kappa})u_1''\psi\} \\ & +\frac{\mu}{\mu_s^0}\{(\lambda_s'^0 + \tfrac{4}{3}\mu_s'^0)(v_1'\psi)' + (\lambda_s'^0 - \tfrac{2}{3}\mu_s'^0)[\phi_1(u' + \mathrm{i}kw)]' \\ & +\mu_s'^0[2(\phi_1 u')' + \mathrm{i}k\phi_1(w' + \mathrm{i}ku)]\}, \end{aligned} \tag{B 9b}$$

$$\begin{aligned} r_{32}^y = {} & F\phi_1 v_1 w' + \tfrac{1}{2}B_0''\phi_1^2(\rho - w) - \mathrm{i}k\tfrac{1}{2}G_0''\phi_1^2\psi + \frac{\mu}{\mu_s^0}\{\mathrm{i}k(\lambda_s''^0 - \tfrac{2}{3}\mu_s''^0)[\phi_1 v_1'\psi \\ & +\tfrac{1}{2}\phi_1^2(u' + \mathrm{i}kw)] + \tfrac{1}{2}\mu_s''^0\{[\phi_1^2(w' + \mathrm{i}ku)]' - 2k^2\phi_1^2 w\}\}, \end{aligned} \tag{B 10a}$$

$$\begin{aligned} r_{32}^z = {} & [Fv_1 v_1' + B_0''\phi_1(u_1 - v_1) + \tfrac{1}{2}B_0'''\phi_1^2]\psi + F\phi_1(v_1 u)' + \tfrac{1}{2}B_0''\phi_1^2(\eta - u) \\ & -\tfrac{1}{2}G_0''(\phi_1^2\psi)' + \frac{\mu}{2\mu_s^0}\{2(\lambda_s''^0 + \tfrac{4}{3}\mu_s''^0)(\phi_1 v_1'\psi)' \\ & +(\lambda_s''^0 - \tfrac{2}{3}\mu_s''^0)[\phi_1^2(u' + \mathrm{i}kw)]' + \mu_s''^0[2(\phi_1^2 u')' + \mathrm{i}k\phi_1^2(w' + \mathrm{i}ku)]\}, \end{aligned} \tag{B 10b}$$

and

$$\begin{aligned} r_{41}^y = {} & -F\delta\phi_1\dot{\rho} - F\delta[\phi_0 u_1 + (1-\omega)\phi_1]\rho' - B_0'\phi_1(\rho - w) - \mathrm{i}k\phi_1 q \\ & +\alpha_2 v\mu\phi_1[\rho'' - k^2\rho + \mathrm{i}k\bar{\kappa}(\eta' + \mathrm{i}k\rho)], \end{aligned} \tag{B 11a}$$

$$\begin{aligned} r_{41}^z = {} & -F\delta\phi_1\dot{\eta} - F\delta\phi_0 u_1'\eta - F\delta[\phi_0 u_1 + (1-\omega)\phi_1]\eta' - F\delta[\dot{u}_1 + (1-\omega)u_1']\psi \\ & -B_0'\phi_1(\eta - u) - [B_0'(u_1 - v_1) + B_0''\phi_1]\psi - p_1'\psi - \phi_1 q' \\ & +\alpha_2 v\mu\{\phi_1[\eta'' - k^2\eta + \bar{\kappa}(ik\rho + \eta')'] + (1+\bar{\kappa})u_1''\psi\}, \end{aligned} \tag{B 11b}$$

$$r_{42}^y = -F\delta\phi_1 u_1\rho' - \tfrac{1}{2}B_0''\phi_1^2(\rho - w), \tag{B 12a}$$

$$r_{42}^z = -[F\delta u_1 u_1' + B_0''\phi_1(u_1 - v_1) + \tfrac{1}{2}B_0'''\phi_1^2]\psi - F\delta\phi_1(u_1\eta)' - \tfrac{1}{2}B_0''\phi_1^2(\eta - u). \tag{B 12b}$$

Using (2.6*a*, *b*) to eliminate v_1', u_1' in favour of $\dot{\phi}_1$, ϕ_1', and (3.16), (3.17) to eliminate w, ρ in favour of u', η', $\dot{\psi}$, ψ', then r_ψ can be written as

$$\begin{aligned} r_\psi = {} & \{[B_0'(u_1 - v_1) + B_0''\phi_1 + p_1']\psi\}' + k^2\phi_0 G_0'\phi_1\psi - \phi_0 G_0'(\phi_1\psi)'' + (\phi_1 q')' - k^2\phi_1 q \\ & +(\beta_1 + v_3k^2)\phi_1'\eta - \left(\beta_2 + 2\frac{\mu}{\mu_s^0}\phi_0\mu_s'^0k^2\right)\phi_1'u - \beta_3(u_1\psi)' - \beta_4(v_1\psi)' \\ & -2F[\phi_0 v_1 + \delta(1-\phi_0)u_1]\dot{\psi}' + 2F[\phi_0\omega v_1 - \delta(1-\phi_0)(1-\omega)u_1]\psi'' \\ & -2F\phi_0[(\dot{\phi}_1 - \omega\phi_1')u]' - 2F\delta(1-\phi_0)\{[\dot{\phi}_1 + (1-\omega)\phi_1']\eta\}' \end{aligned}$$

$$+[(F\tilde{H}u_1+c\phi_0 v_1)\psi]'''+[(F\tilde{H}\eta+c\phi_0 u)\phi_1']''+\beta_5(\phi_1\dot{\psi})''-\beta_6(\phi_1\psi')''$$
$$+(\beta_7-\beta_{12}k^2)\phi_1\dot{\psi}+(\beta_8-\beta_{13}k^2)\phi_1\psi'+\beta_9\dot{\phi}_1\dot{\psi}+\beta_{10}(\dot{\phi}_1\psi'+\phi_1'\dot{\psi})$$
$$+\beta_{11}\phi_1'\psi'+\frac{v_3}{\phi_0}A+\frac{\mu}{\mu_s^0}\frac{\phi_0}{1-\phi_0}B+O(\phi_1^2), \tag{B 13}$$

with

$$v_3=v\mu[\alpha_1\phi_0+\alpha_2(1-\phi_0)], \tag{B 14}$$

the additional types of terms due to $\alpha_{1,2}$,

$$A=-\phi_0\phi_1'\eta''+(1+\bar{\kappa})\{[\dot{\phi}_1+(1-\omega)\phi_1']'\psi\}'+\phi_1[\dot{\psi}+(1-\omega)\psi']''$$
$$+\bar{\kappa}\{\phi_1[\dot{\psi}+(1-\omega)\psi']'\}', \tag{B 15}$$

due to the variable viscosity,

$$B=-k^2(\lambda_s'^0-\tfrac{2}{3}\mu_s'^0)(\dot{\phi}_1-\omega\phi_1')\psi+2\mu_s'^0(1-\phi_0)(\phi_1'u')'+2\mu_s'^0[\phi_1(\dot{\psi}-\omega\psi')']'$$
$$+(\lambda_s'^0-\tfrac{2}{3}\mu_s'^0)[\phi_1(\dot{\psi}-\omega\psi')]''+(\lambda_s'^0+\tfrac{4}{3}\mu_s'^0)[(\dot{\phi}_1-\omega\phi_1')\psi]'', \tag{B 16}$$

and the various coefficients

$$\left.\begin{aligned}
&\beta_1=B_0'-\beta_3,\ \beta_2=B_0'+\beta_4,\ \beta_3=F[E(1-\phi_0)+\tilde{H}k^2],\ \beta_4=\phi_0(FE+ck^2),\\
&\beta_5=\frac{c\phi_0}{1-\phi_0}-\frac{F\tilde{H}}{\phi_0}=\frac{F(\tilde{J}\phi_0-\tilde{H})}{\phi_0(1-\phi_0)},\ \beta_6=\frac{c\phi_0\omega}{1-\phi_0}+\frac{F\tilde{H}(1-\omega)}{\phi_0}=\beta_5\omega+\frac{F\tilde{H}}{\phi_0},\\
&\beta_7=-\left(\frac{\beta_1}{\phi_0}+\frac{\beta_2}{1-\phi_0}\right)=\frac{1}{\phi_0(1-\phi_0)}\left[FE(1-2\phi_0)-B_0'-F(\tilde{J}\phi_0-\tilde{H})k^2\right],\\
&\beta_8=\frac{\omega\beta_2}{1-\phi_0}-\frac{1-\omega}{\phi_0}\beta_1,\ \beta_9=2F\frac{\delta(1-\phi_0)^2-\phi_0^2}{\phi_0(1-\phi_0)},\\
&\beta_{10}=\frac{2F}{\phi_0(1-\phi_0)}[\phi_0^2\omega+\delta(1-\phi_0)^2(1-\omega)],\\
&\beta_{11}=\frac{2F}{\phi_0(1-\phi_0)}[\delta(1-\phi_0)^2(1-\omega)^2-\phi_0^2\omega^2],\ \beta_{13}=v_3\frac{1+\bar{\kappa}}{\phi_0}-\beta_{12}\omega,\\
&\beta_{12}=v_3\frac{1+\bar{\kappa}}{\phi_0}+\frac{\mu}{\mu_s^0}\frac{\phi_0}{1-\phi_0}(\lambda_s'^0+\tfrac{4}{3}\mu_s'^0).
\end{aligned}\right\} \tag{B 17}$$

The terms proportional to $\exp(\mathrm{i}\lambda z)$ follow as given in (3.20*a*), with

$$\left.\begin{aligned}
\gamma_1&=\phi_0G_0'(\lambda^2+k^2)-a\lambda^2+\frac{\mathrm{i}\lambda}{\phi_0}[\phi_0B_0''+F\tilde{H}\lambda^2-\beta_1-v_3(1+\bar{\kappa})\lambda^2]\\
&\quad+(\sigma-\mathrm{i}\lambda\omega)\left[\beta_7-(\beta_5+\beta_{12})\lambda^2-\frac{\mu}{\mu_s^0}\frac{\phi_0}{1-\phi_0}(\lambda_s'^0-\tfrac{2}{3}\mu_s'^0)k^2\right],\\
\gamma_2&=\beta_7-\beta_5\lambda^2-\beta_{12}k^2+\sigma\beta_9+\mathrm{i}\lambda\beta_{10}-\frac{\mu}{\mu_s^0}\frac{\phi_0}{1-\phi_0}(\lambda_s'^0-\tfrac{2}{3}\mu_s'^0)\lambda^2,\\
\gamma_3&=\mathrm{i}\lambda(\beta_1-F\tilde{H}\lambda^2+v_3k^2)-2\mathrm{i}\lambda F\delta(1-\phi_0)[\sigma+\mathrm{i}\lambda(1-\omega)],\\
\gamma_4&=-\mathrm{i}\lambda\left(\beta_2+c\phi_0\lambda^2+2\frac{\mu}{\mu_s^0}\mu_s'^0\phi_0k^2\right)-2\mathrm{i}\lambda F\phi_0(\sigma-\mathrm{i}\lambda\omega).
\end{aligned}\right\} \tag{B 18}$$

Obviously, the terms $\sim \exp(-\mathrm{i}\lambda z)$ are obtained by substituting the coefficients of the perturbation variables by their complex conjugates; this gives r_-. Making use of

(3.4*b*, *c*), the constant terms (with respect to z) enter r_0 as described in (3.20*c*), where

$$\left.\begin{aligned}
&\gamma_5 = \beta_1 + \nu_3(\lambda^2+k^2), \quad \gamma_6 = \beta_2 + 2\frac{\mu}{\mu_s^0}\mu_s'^0\phi_0 k^2,\\
&\gamma_7 = \beta_7 - \beta_{12}k^2 - \frac{\nu_3}{\phi_0}\lambda^2, \quad \gamma_8 = k^2\tilde{\gamma}_9 + \mathrm{i}\lambda\tilde{\gamma}_8,\\
&\tilde{\gamma}_8 = \beta_8 - \beta_{13}k^2 - \frac{\nu_3}{\phi_0}(1-\omega)\lambda^2, \quad \tilde{\gamma}_9 = \phi_0 G_0' - (\sigma - \mathrm{i}\lambda\omega)(\lambda_s'^0 - \tfrac{2}{3}\mu_s'^0).
\end{aligned}\right\} \tag{B 19}$$

Appendix C

In §3.3, the pressure coefficients $c_q^{\pm}$, $\tilde{c}_q^{\pm}$, c_q^0, follow directly from (3.21) upon replacing $\ddot{\psi}_{\pm}$ by the leading approximations of (3.19):

$$\left.\begin{aligned}
&c_q^+ = a_4 - \frac{Fa_2}{A(1-\phi_0)(\lambda^2+k^2)} = \overline{c_q^-}, \ \tilde{c}_q^+ = a_5 - \frac{Fa_3}{A(1-\phi_0)(\lambda^2+k^2)} = \overline{\tilde{c}_q^-},\\
&c_q^0 = -(1-\delta)\frac{EF}{Ak^2} + \frac{1}{A}\left(\delta c - \nu\mu\frac{1+\bar{\kappa}}{\phi_0}[1-(1-\phi_0)(\alpha_2-\alpha_1\delta)]\right), \ \tilde{c}_q^0 = -\delta\frac{G_0}{A}.
\end{aligned}\right\} \tag{C 1}$$

The velocity coefficients like c_u^+, stemming from the 'expansion' (3.28) with respect to ψ_+ and $\dot{\psi}_+$ read

$$\left.\begin{aligned}
&c_u^+ = \frac{\rho_6\zeta_6 - \rho_8\zeta_5}{\rho_6\rho_7 - \rho_5\rho_8} = \overline{c_u^-}, \quad \tilde{c}_u^+ = \frac{\rho_7\zeta_5 - \rho_5\zeta_6}{\rho_6\rho_7 - \rho_5\rho_8} = \overline{\tilde{c}_u^-},\\
&c_\eta^+ = \frac{1}{a_{62}}[\rho_1 c_u^+ + F(1-\phi_0)\tilde{c}_u^+ - \zeta_1] = \overline{c_\eta^-}, \quad \tilde{c}_\eta^+ = \frac{1}{a_{62}}[\rho_2 c_u^+ + a_{61}\tilde{c}_u^+ - \zeta_2] = \overline{\tilde{c}_\eta^-},
\end{aligned}\right\} \tag{C 2}$$

where

$$\left.\begin{aligned}
&\rho_1 = a_{61} - F(1-\phi_0)a_2/A, \qquad \rho_2 = -F(1-\phi_0)a_3/A,\\
&\rho_3 = a_8 - F\delta\phi_0 a_2/A, \qquad \rho_4 = F\delta\phi_0 a_3/A,\\
&\zeta_1 = \mathrm{i}\lambda[\mu_1 - (1-\phi_0)c_q^+], \qquad \zeta_2 = a_7 - \mathrm{i}\lambda(1-\phi_0)\tilde{c}_q^+,\\
&\zeta_3 = -\mathrm{i}\lambda\left(\nu_2\frac{\bar{\kappa}}{\phi_0} + \phi_0 c_q^+\right), \qquad \zeta_4 = -(a_9 + \mathrm{i}\lambda\phi_0\tilde{c}_q^+);\\
&\rho_5 = \rho_1\rho_3 + F\delta\phi_0\rho_2 - B_0 a_{62}, \qquad \rho_6 = F(1-\phi_0)\rho_3 + F\delta\phi_0 a_{61},\\
&\rho_7 = a_8\rho_2 - \rho_1\rho_4, \qquad \rho_8 = a_{61}a_8 - F(1-\phi_0)\rho_4 - B_0 a_{62},\\
&\zeta_5 = \rho_3\zeta_1 + F\delta\phi_0\zeta_2 + a_{62}\zeta_3, \qquad \zeta_6 = a_8\zeta_2 + a_{62}\zeta_4 - \rho_4\zeta_1.
\end{aligned}\right\} \tag{C 3}$$

They have been determined by inserting the ansatz (3.28) into (3.22*a*) and (3.23*a*), which gives, e.g. from (3.22*a*),

$$\begin{aligned}
&\dot{\psi}_+\left\{\left[a_{61} - F(1-\phi_0)\frac{a_2}{A}\right]c_u^+ + F(1-\phi_0)\tilde{c}_u^+ - a_{62}c_\eta^+ + \mathrm{i}\lambda(1-\phi_0)c_q^+ - \mathrm{i}\lambda\mu_1\right\}\\
&+\psi_+\left\{-F(1-\phi_0)\frac{a_3}{A}c_u^+ + a_{61}\tilde{c}_u^+ - a_{62}\tilde{c}_\eta^+ - a_7 + \mathrm{i}\lambda(1-\phi_0)\tilde{c}_q^+\right\} = O(\phi_\pm),
\end{aligned}$$

and treating ψ_+ and $\dot{\psi}_+$ as sorts of linearly independent basis functions, so that within the considered approximation the coefficients in the last equation must vanish. This gives two linear relations for the four coefficients sought c_u^+, $\tilde{c}_u^+$, c_η^+, $\tilde{c}_\eta^+$; the other two follow from insertion of (3.28) into (3.23*a*). The coefficients with the zero index, like c_u^0, c_η^0, etc., follow upon setting $\lambda = 0$ in (C 2) and (C 3).

The coefficients θ_i occurring in (3.29) follow from inserting (3.28) into the expres-

sions (3.20a, c) for r_+ and r_0; thus

$$\left.\begin{aligned}
&\theta_1 = F^{-1}(\gamma_2 + \gamma_3 c_\eta^0 + \gamma_4 c_u^0 - k^2 c_q^0), \quad \theta_2 = F^{-1}(\gamma_1 + \gamma_3 \tilde{c}_\eta^0 + \gamma_4 \tilde{c}_u^0 - k^2 \tilde{c}_q^0),\\
&\theta_3 = F^{-1}[\gamma_7 - k^2 c_q^+ + \mathrm{i}\lambda(\gamma_6 c_u^+ - \gamma_5 c_\eta^+)],\\
&\theta_4 = F^{-1}[\gamma_8 - k^2 \tilde{c}_q^+ + \mathrm{i}\lambda(\gamma_6 \tilde{c}_u^+ - \gamma_5 \tilde{c}_\eta^+)].
\end{aligned}\right\} \tag{C 4}$$

Appendix D

The coefficient χ of (4.12) follows from substituting

$$\hat{w}_+ = \mathrm{i}\hat{k}\delta_3\tilde{\psi}_+, \quad \hat{\rho}_+ = \mathrm{i}\hat{k}\delta_4\tilde{\psi}_+; \quad (\hat{w}, \hat{\rho})_- = \mathrm{i}\hat{k}(\bar{\delta}_3, \bar{\delta}_4)\tilde{\psi}_-, \tag{D 1}$$

where

$$\delta_3 = \frac{a_8^0\delta_1 + a_{62}^0\delta_2}{B_0 a_{62}^0 - a_{61}^0 a_8^0}, \quad \delta_4 = \frac{B_0\delta_1 + a_{61}^0\delta_2}{B_0 a_{62}^0 - a_{61}^0 a_8^0}, \tag{D 2}$$

$$\delta_1 = G_0 + (1-\phi_0)a_5^0 + \mathrm{i}\lambda\mu_2, \quad \delta_2 = \phi_0 a_5^0 + \mathrm{i}\lambda(1-\omega)v_2\frac{\bar{\kappa}}{\phi_0} \tag{D 3}$$

upon solving (4.11), so that

$$\chi = \phi_0 G_0' - a_5^0 + B_0'(\delta_3 - \delta_4) + FE[\phi_0\delta_3 + (1-\phi_0)\delta_4] - v_3\left[\lambda^2\delta_4 + \mathrm{i}\lambda\bar{\kappa}\frac{1-\omega}{\phi_0}\right]. \tag{D 4}$$

The coefficients χ_i appearing in equations (4.16)–(4.19) stem from writing the dispersion relation (4.13) in the alternative form

$$\hat{\tau}^4 + \chi_1\hat{k}^2\hat{\tau}^3 + \chi_2\hat{k}^4\hat{\tau}^2 + (\chi_3\hat{k}^4 - \chi_5)\hat{k}^2\hat{\tau} + (\chi_4\hat{k}^4 - \chi_6)\hat{k}^4 = 0, \tag{D 5}$$

so that

$$\left.\begin{aligned}
&\chi_1 = \tilde{\mu} + \xi_1 + 2\xi_2, \quad \chi_2 = \tilde{\mu}(\xi_1 + 2\xi_2) + \xi_2^2 + \xi_3^2 + 2\xi_1\xi_2,\\
&\chi_3 = \tilde{\mu}(\xi_2^2 + \xi_3^2 + 2\xi_1\xi_2) + \xi_1(\xi_2^2 + \xi_3^2), \quad \chi_4 = \tilde{\mu}\xi_1(\xi_2^2 + \xi_3^2),\\
&\chi_5 = \frac{2\lambda_0\xi_5}{F(1-\phi_0+\delta\phi_0)}, \quad \chi_6 = \frac{2\lambda_0}{F(1-\phi_0+\delta\phi_0)}(\xi_2\xi_5 - \xi_3\xi_4).
\end{aligned}\right\} \tag{D 6}$$

REFERENCES

Anderson, T. B. & Jackson, R. 1968 Fluid mechanical description of fluidized beds. *Ind. Eng. Chem. Fundam.* **7**, 12–21.

Anderson, K., Sundaresan, S. & Jackson, R. 1995 Instabilities and the formation of bubbles in fluidized beds. *J. Fluid Mech.* **303**, 327–366.

Batchelor, G. K. 1993 Secondary instability of a gas-fluidized bed. *J. Fluid Mech.* **257**, 359–371.

Batchelor, G. K. & Nitsche, J. M. 1991 Instability of stationary unbounded stratified fluid. *J. Fluid Mech.* **227**, 357–391.

Didwania, A. K. & Homsy, G. M. 1981 Flow regimes and flow transitions in liquid fluidized beds. *Intl J. Multiphase Flow* **7**, 563–580.

El-Kaissy, M. M. & Homsy, G. M. 1976 Instability waves and the origin of bubbles in fluidized beds. Part I: experiments. *Intl J. Multiphase Flow* **2**, 379–395.

Garg, S. K. & Pritchett, J. W. 1975 Dynamics of gas-fluidized beds. *J. Appl. Phys.* **46**, 4493–4500.

Glasser, B. J. 1996 One- and two-dimensional travelling wave solutions in fluidized beds. PhD Dissertation, Princeton University.

Glasser, B. J., Kevrekidis, I. G. & Sundaresan, S. 1996 One- and two-dimensional travelling wave solutions in gas-fluidized beds. *J. Fluid Mech.* **306**, 183–221.

GLASSER, B. J., KEVREKIDIS, I. G. & SUNDARESAN, S. 1997 Fully developed travelling wave solutions and bubble formation in fluidized beds. *J. Fluid Mech.* **334**, 157–188.

GÖZ, M. F. 1992 On the origin of wave patterns in fluidized beds. *J. Fluid Mech.* **240**, 379–404.

GÖZ, M. F. 1993*a* Instabilities and the formation of wave patterns in fluidized beds. In *Instabilities in Multiphase Flows* (ed. G. Gouesbet & A. Berlemont), pp. 251–259. Plenum.

GÖZ, M. F. 1993*b* Bifurcation of plane voidage waves in fluidized beds. *Physica* D **65**, 319–351.

GÖZ, M. F. 1995*a* Quasi-stationary instabilities in fluidized beds. *Phys. Lett.* A **200**, 355–359.

GÖZ, M. F. 1995*b* Small Froude number asymptotics in two-dimensional two-phase flows. *Phys. Rev.* E **52**, 3697–3710.

GÖZ, M. F. 1995*c* Transverse instability of plane wavetrains in gas-fluidized beds. *J. Fluid Mech.* **303**, 55–81.

GÖZ, M. F., GLASSER, B. J., KEVREKIDIS, I. G. & SUNDARESAN, S. 1996 Traveling waves in multiphase flows. In *Advances in Fluid Mechanics* (ed. M. Rahman & C. A. Brebbia), pp. 307–316. Comp. Mech. Publ.

HERNÁNDEZ, J. A. & JIMÉNEZ, J. 1991 Bubble formation in dense fluidized beds. In *Proc. NATO Advanced Research Workshop on the Global Geometry of Turbulence* (ed. J. Jiménez), pp. 133–142. Plenum.

KOMATSU, T. S. & HAYAKAWA, H. 1993 Nonlinear waves in fluidized beds. *Phys. Lett.* A **183**, 56–62.

KUIPERS, J. A. M., PRINS, W. & SWAAIJ, W. P. M. VAN 1991 Theoretical and experimental bubble formation at a single orifice in a two-dimensional gas-fluidized bed. *Chem. Engng Sci.* **46**, 2881–2894.

NEEDHAM, D. J. & MERKIN, J. H. 1986 The existence and stability of quasi-steady periodic voidage waves in a fluidized bed. *Z. Angew. Math. Phys.* **37**, 322–339.

NICOLAS, M., CHOMAZ, J.-M., VALLET, D. & GUAZZELLI, E. 1996 Experimental investigations on the nature of the first wavy instability in liquid-fluidized beds. *Phys. Fluids* **8**, 1987–1989 (L).

PRITCHETT, J. W., BLAKE, T. R. & GARG, S. K. 1978 A numerical model of gas fluidized beds. *AIChE Symp. Series 176*, vol. 74, pp. 134–148.

RICHARDSON, J. F. & ZAKI, W. N. 1954 Sedimentation and fluidization: Part I. *Trans. Inst. Chem. Engrs* **32**, 35–53.

WANG, C.-H., JACKSON, R. & SUNDARESAN, S. 1996 Stability of bounded rapid shear flows of a granular material. *J. Fluid Mech.* **308**, 31–62.

WILHELM, R. H. & KWAUK, M. 1948 Fluidization of solid particles. *Chem. Engng Prog.* **44**, 201–218.